NUCLEAR MEDICINE AND MOLECULAR IMAGING

Annual Report

2007

University Medical Center Groningen

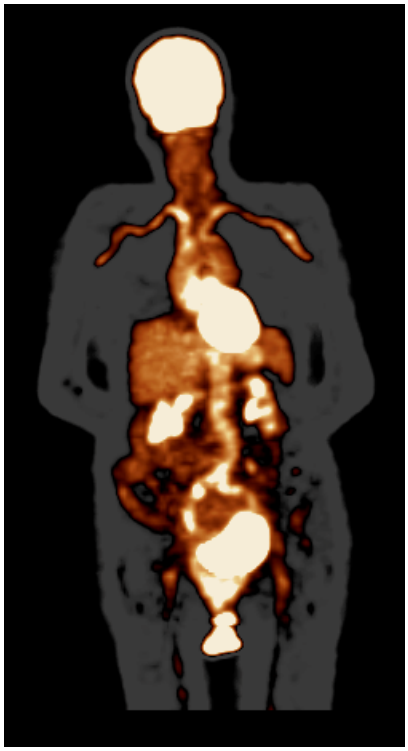

umcg

Nuclear Medicine and Molecular Imaging

Annual Report 2007

Nuclear Medicine and Molecular Imaging
University Medical Center Groningen
P.O.Box 30001
9700 RB Groningen
The Netherlands

Cover illustration: FDG-whole body scan of a patient with vasculitis. A marked tracer uptake is observed in the major blood vessels, which is lacking in healthy normal subjects. Image provided by dr.R.H.J.A.Slart.

EDITORS: A.van Waarde
A.M.J.Paans

CONTENTS

CLINICAL APPLICATIONS

As in the previous years, the number of nuclear medicine studies was increased in 2007 as compared to 2006, with an overall percentage of 4 %. The total production of the Department of Nuclear Medicine and Molecular Imaging was increased by 29% between 2003 and 2007.

The number of studies with single photon emitters was increased by 3% in 2007. For studies with positron emitters, the increase was almost 9%, mainly due to a steady increase of the demand for FDG-PET and a revival of ^{13}N-ammonia studies of the heart. Details are presented in Tables 1 and 2.

Three developments are evident: (i) there seems to be a gradual shift from SPECT towards PET; (ii) some well-established diagnostic tools are being replaced by other techniques, often from other disciplines than nuclear medicine, which makes nuclear medicine a dynamic field; (iii) an increasing number and an increasing diversity of radiopharmaceuticals is being employed, whereas new indications for old radiopharmaceuticals do also appear. The dynamics of the nuclear medicine environment in Groningen will probably be further enhanced by the planned acquisition of novel imaging equipment.

When we look at Tables 1 and 2 in more detail, the following developments can be noticed:

1. A gradual decline of lung perfusion scintigraphy since 2005. This decline is caused predominantly by the ascent of multislice CT as the diagnostic tool in patients with pulmonary embolism. At the time of this writing, the national discussion on the place of perfusion scintigraphy in the diagnosis of pulmonary embolism has not yet been completed, but most likely the position of CT will be strengthened. A further decline of lung perfusion scintigraphy will then take place in the near future. Since the radiation dose of CT is quite high, young women run an increased risk for the development of mammary carcinoma. This undesired side effect may result in a continued demand for lung perfusion scintigraphy in this patient group, although the magnitude of this demand can not yet be estimated.

2. A decrease of the number of myocardial scintigraphy scans. Since there is no explanation for this decline, it appears to be a normal yearly fluctuation. Based on epidemiological data, one would have expected a steady-state or a slight increase of the demand for these scans.

3. A continous rise of the amount of bone densitometry scans (by 54% since 2003). This probably reflects aging of the population, with a corresponding increase of the risk for osteoporosis.

4. A sharp decline of the number of 37 and 74 MBq ^{131}I scans in patients with thyroid cancer. This is probably due to the fact that the 74 MBq scans have been deleted from the national consensus protocol for a number of indications. A further

decrease of the number of 74 MBq scans may be expected in the near future when the new protocol is fully in operation.

5. For about three decennia, the UMCG has assessed glomerular filtration rate (GFR) and effective renal plasma flow (ERPF) using ^{125}I-iothalamate and ^{131}I-hippuran. Around 900 of such studies were performed each year. Recently it was proven that algorithms estimating clearance show large deviations from this golden standard. Yet, it is hard to maintain and expand the unique database that the UMCG has created, since industry fails to provide us with the necessary radiopharmaceuticals.

6. Two methods for assessment of the presynaptic dopaminergic status are available in our department, viz. ^{123}I-FP-CIT SPECT and ^{18}F-FDOPA-PET. The use of the SPECT-technique has been increased recently, whereas the PET technique has shown a decline. FP-CIT appears to be a good alternative for FDOPA in a clinical setting. Thus, FDOPA-PET is used less often in Parkinsonian patients and more often in patients with neuro-endocrine tumours. It is hard to predict what the future will bring in these areas.

7. Liver and spleen scintigraphy seems to disappearing. In former years, this nuclear medicine technique was an integral part of the liver transplantation program, but it has now been replaced by CT, MRI and ultrasound.

8. The demand for octreotide scintigraphy has decreased sharply, with a corresponding increase in the number of FDOPA scans in patients with neuro-endocrine tumours. The combined number of octreotide, FDOPA and ^{11}C-HTP scans has increased substantially. This rise is related to ongoing research projects, and to the position of our Department as a referral centre for the Netherlands, and part of northern Germany.

9. The demand for ^{11}C-raclopride scans has risen steeply in 2007 because of the fact that novel research projects were initiated which will be continued in the forthcoming years.

Table 1. Studies with single photon emitters performed in 2003 - 2007

			radiopharmaceutical	2003	2004	2005	2006	2007
LUNGS								
305312D	Lung perfusion scintigraphy		^{99m}Tc-MAA	529	608	702	624	456
305312K	Lung ventilation scintigraphy		^{81m}Kr	177	222	247	197	187
305312E	Aspiration scintigraphy		^{99m}Tc-colloid	2	19	8	2	3
		subtotal		**708**	**849**	**957**	**823**	**646**
HEART, VESSELS								
303014D	Myocardial scintigraphy rest		^{99m}Tc-tetrofosmin	799	815	884	1061	975
303015D	Myocardial scintigraphy exercise		^{99m}Tc-tetrofosmin	155	194	271	272	295
303016D	Myocardial scintigraphy adenosine		^{99m}Tc-tetrofosmin	630	619	610	777	682
303054P	Myocardial metabolism FDG SPECT		^{18}F-FDG	42	30	36	37	29
303134E	MUGA-rest		^{99m}Tc-pertechnetate	607	654	618	666	814
303134F	MUGA-first pass (extra)		^{99m}Tc-pertechnetate	82	101	128	368	311
303314D	Right-toleft/left-to-right shunting		^{99m}Tc-MAA/^{99m}Tc-MDP	6	6	1	8	4
303032J	Myocardial innervation		^{123}I-MIBG	0	0	0	0	12
		subtotal		**2321**	**2419**	**2548**	**3189**	**3122**
SKELETON								
304011B	Skeletal scintigraphy detail (flow + blood pool)		^{99m}Tc-MDP	95	162	161	182	256
304012B	Skeletal scintigraphy detail		^{99m}Tc-MDP	304	322	438	376	455
304022B	Skeletal scintigraphy total body		^{99m}Tc-MDP	834	909	780	792	861
304360D	Bone densitometry lower arm			1132	1445	1508	1689	1816
304360E	Bone densitometry lumbar vertebral column			1213	1490	1542	1702	1825
304360F	Bone densitometry hip			1196	1485	1538	1695	1826
304360H	Bone densitometry total body			3	0	15	39	24
		subtotal		**4777**	**5813**	**5982**	**6475**	**7063**

ENDOCRINOLOGY							
301012I	Thyroid scintigraphy	^{123}I	99	118	112	125	106
301022K	Thyroid cancer scintigraphy	^{131}I (1-2 mCi)	55	52	78	66	39
301022N	Posttherapy scanning	^{131}I	37	80	82	61	46
301062K	Thyroid uptake	^{131}I	74	74	80	68	75
301132A	Parathyroid scintigraphy	^{99m}Tc-MIBI/^{123}I	41	40	46	32	37
301022D	DMSA-V total body	^{99m}Tc-DMSA-V	3	12	4	4	6
301222I	Adrenal marrow scintigraphy	^{123}I-MIBG	29	30	37	54	62
301312J	Adrenal cortex scintigraphy	^{131}I-methylnorcholesterol	1	1	0	0	1
	subtotal		**339**	**407**	**439**	**410**	**372**
UROGENITAL SYSTEM							
307031F	Renography	^{99m}Tc-MAG3	123	75	58	48	40
307031G	Renography + furosemide	^{99m}Tc-MAG3	123	106	117	130	138
307031N	Renography + captopril	^{99m}Tc-MAG3	6	7	7	2	2
307031T	Renography of renal transplant	^{99m}Tc-MAG3	34	37	47	32	25
307032D	Renal scintigraphy	^{99m}Tc-DMSA	139	127	141	106	133
307170Y	Clearance studies ERPF/GFR	^{125}I-iothalamate/^{131}I-hippuran	795	1021	820	857	983
	subtotal		**1220**	**1373**	**1190**	**1175**	**1321**
CENTRAL NERVOUS SYSTEM							
300012B	Cisternography	^{111}In-DTPA	0	0	1	2	5
300111C	Liquor drain function	^{111}In-DTPA	0	0	4	2	0
300252M	DAT-scan	^{123}I-FP-CIT	23	38	9	19	53
	subtotal		**23**	**38**	**14**	**23**	**58**

DIGESTIVE TRACT							
306131B	Oesophagus scintigraphy	^{99m}Tc-colloid	97	75	62	80	62
306231A	Gastric scintigraphy/Meckel's diverticulum	^{99m}Tc-sodiumpertechnetate	7	6	7	6	3
306231B	Gastric emptying	^{99m}Tc-sodiumpertechnetate	53	62	63	121	124
306512C	Liver and spleen scintigraphy	^{99m}Tc-colloid	87	70	64	42	16
306631H	Bile duct scintigraphy	^{99m}Tc-mebrofenin	43	34	24	22	22
	Miscellaneous		3	3	1	2	1
	subtotal		**290**	**250**	**221**	**273**	**228**
BLOOD, INFECTION, TUMOR							
302232E	Sentinal node scintigraphy	^{99m}Tc-nanocolloid	139	123	171	159	176
301231S	Octreotide scintigraphy	^{111}In-octreotide	51	72	63	83	47
309052	Tumor localisation (general)		11	16	15	3	3
302070L	Plasma volume assessment	^{125}I-albumin	10	10	11	13	7
302070O	Erythrocyte volume assessment	^{51}Cr-autologous erythrocytes	10	10	11	13	7
302222	Lymph scintigraphy	^{99m}Tc-nanocolloid	13	26	18	13	15
302422C	Bone marrow scintigraphy	^{99m}Tc-nanocolloid	3	6	1	5	6
302622H	Infection diagnostics (whole body)	^{99m}Tc-leukocytes	80	95	85	68	86
304012H	Infection diagnostics (detail)	^{99m}Tc-leukocytes	17	32	35	36	52
302622O	Infection diagnostics	^{67}Ga-citrate	32	13	2	0	1
306370O	Schilling test	^{57}Co-cyanocobolamin	57	14	55	37	15
306370P	Schilling test with intrinsic factor	^{57}Co-cyanocobolamin	7	1	2	8	1
	Miscellaneous		1	2	0	0	1
	subtotal		**431**	**420**	**469**	**438**	**417**
MISCELLANEOUS							
300411B	Lacrimal duct scintigraphy	^{99m}Tc-pertechnetate	60	7	1	4	1
309000	Asessment of leakage during intraoperative chemotherapy	^{131}I-HSA	11	11	6	15	8
309042I	Amyloidscintigrafie	^{123}I-SAP	51	58	57	41	56
	subtotal		**122**	**76**	**64**	**60**	**65**

THERAPY							
301000K	Thyroid carcinoma	^{131}I	47	81	80	66	53
301000L	Hyperthyroidism	^{131}I	77	85	90	83	73
301200J	Neuroendocrine tumors	^{131}I-MIBG	0	0	4	2	5
302400P	Polycytaemia vera	^{32}P	9	7	10	7	5
304000Z	Metastatic bone disease	^{89}Sr-chloride	11	10	10	5	6
304100Y	Arthritis/synovitis	^{90}Y	1	2	4	0	4
	subtotal		**145**	**185**	**198**	**163**	**146**
	total single photon		**10376**	**11830**	**12082**	**13029**	**13438**
	index (2003 = 100%)		**100**	**114**	**116**	**126**	**130**

Table 2. Studies with positron emitters performed in 2003 - 2007

CENTRAL NERVOUS SYSTEM							
940021		^{11}C-methionine	6	24	31	26	56
940037		^{11}C-raclopride	23	18	32	3	39
940202		^{15}O-H_2O	236	264	85	36	20
940.310		^{18}F-FDG	109	109	132	149	127
940311		^{18}F-FDOPA	92	100	46	60	34
948000		^{11}C-verapamil	5	1	35	26	4
	subtotal		**471**	**516**	**361**	**300**	**280**
HEART, VESSELS							
941103	Myocardial perfusion	^{13}N-NH_3	157	205	49	74	141
941310	Viability	^{18}F-FDG	55	81	28	36	38
941.062	Miscellaneous		5	4	0	0	0
	subtotal		**217**	**290**	**77**	**110**	**179**
BLOOD, INFECTION, TUMOR							
947310	Whole body scanning	^{18}F-FDG	1207	1436	1453	1574	1712
947335	Whole body scanning	^{18}F-FLT	48	33	14	11	20
947021	Whole body scanning	^{11}C-methionine	6	3	6	19	14
947311	Whole body scanning	^{18}F-FDOPA	15	68	115	152	182
947370	Whole body scanning	^{18}F-FMISO	1	2	2	0	0
947371	Whole body scanning	^{18}F-NaF	0	25	19	3	2
947610	Whole body scanning	^{124}I	0	0	2	23	3
947710	Whole body scanning	^{89}Zr-Moabs	0	0	0	4	22
947202	Tumor perfusion	^{15}O-H_2O	0	0	0	11	5
946023	Urogenital tract	^{11}C-choline	37	36	46	39	31
	subtotal		**1314**	**1603**	**1657**	**1836**	**1991**

EXPERIMENTAL							
948003		^{11}C-mHED	0	4	0	0	11
948004		^{11}C-SA4503	0	0	4	18	1
948006		^{11}C-HTTP	0	0	6	53	35
948007		^{11}C-PK11195	0	0	3	6	31
948370		^{11}C-ganciclovir	2	7	2	4	0
	subtotal		**2**	**11**	**15**	**81**	**78**
MISCELLANEOUS							
942000		^{11}C-CO_2	0	0	2	0	0
	subtotal		**0**	**0**	**2**	**0**	**0**
	total positron emission		**2004**	**2420**	**2112**	**2327**	**2528**
	index (2003 = 100%)		**100**	**121**	**105**	**116**	**126**
	total single photon + positron emission		**12380**	**14250**	**14194**	**15356**	**15966**
	index (2003 = 100%)		**100**	**115**	**115**	**124**	**129**

CLINICAL RESEARCH

2.1 Cardiology

2.1.1 Measurement of coronary calcium scores or exercise testing as initial screening tool in asymptomatic subjects with ST-T changes on the resting ECG: an evaluation study

In cooperation with Depts. Cardiology, Clinical Pharmacology, Nephrology, Radiology (Groningen) and Dept. Medical Informatics (Erasmus University, Rotterdam)

Asymptomatic subjects at intermediate coronary risk may need diagnostic testing for risk stratification. Both measurement of coronary calcium scores and exercise testing are well established screening methods for this purpose. However, it is not clear which test should be preferred as the initial diagnostic tool. We evaluated the prevalence of documented coronary artery disease (CAD) according to calcium scores and exercise test results.

Asymptomatic subjects with ST-T changes on a rest ECG were selected from the population based PREVEND cohort study and underwent measurement of calcium scores by electron beam tomography and exercise testing. With calcium scores ≥ 10 or a positive exercise test, myocardial perfusion imaging (MPI) or coronary angiography (CAG) was recommended. The primary endpoint was documented obstructive CAD (≥ 50% stenosis).

Of 153 subjects included, 149 subjects completed the study protocol. Calcium scores ≥ 400, 100–399, 10–99 and < 10 were found in 16, 29, 18 and 86 subjects and the primary endpoint was present in 11 (69%), 12 (41%), 0 (0%) and 1 (1%) subjects, respectively. A positive, nondiagnostic and negative exercise test was present in 33, 27 and 89 subjects and the primary endpoint was present in 13 (39%), 5 (19%) and 6 (7%) subjects, respectively. Receiver operator characteristics analysis showed that the area under the curve, as a measure of the diagnostic yield, of 0.91 (95% CI 0.84–0.97) for calcium scores was superior to 0.74 (95% CI 0.64–0.83) for exercise testing ($p = 0.004$).

In conclusion, measurement of coronary calcium scores is an appropriate initial non-invasive test in asymptomatic subjects at increased coronary risk.

2.1.2 Myocardial perfusion falls during hemodialysis

In cooperation with Depts. Nephrology and Cardiology (Groningen), Dialysis Center Groningen, and Dept. Renal Medicine, Derby City General Hospital, Derby, United Kingdom. Supported by an unrestricted grant from Amgen BV

Hemodialysis (HD) patients have highly elevated cardiac mortality rates. The HD procedure is associated with hemodynamic instability and an increased risk of sudden death. Previous studies suggest that HD may elicit myocardial ischemia. However,

the effect of HD on myocardial blood flow has not been quantified. We studied the effect of HD on global and regional myocardial perfusion.

^{13}N-NH_3 Positron Emission Tomography (PET) was used to quantify changes in myocardial perfusion, left ventricular (LV) wall motion, cardiac output (CO), LV end-diastolic (LVEDV), and end-systolic volume (LVESV) in 7 non-hypotension prone HD patients. PET scans were performed before HD and at 30 and 220 min of HD. In all patients myocardial perfusion fell during HD. At 30 min of HD without ultrafiltration (UF), global myocardial perfusion had fallen 13.5±11.5% ($p<0.05$) while CO, LVEDV and LVESV were 4.6±5.3% (NS), 5.6±4.2% ($p<0.05$) and 6.9±7.2% ($p<0.05$) lower, respectively. At 220 min of HD, after UF of 2.5±0.9 l, global myocardial perfusion had fallen 26.6±13.9% ($p<0.05$) from baseline while CO, LVEDV, and LVESV were 21.0±19.7%, 31.1±12.7% and 36.4±17.5% (all $p<0.05$) lower, respectively. In 2 patients, LV regional wall motion abnormalities (RWMA) developed at 220 min. Myocardial perfusion was reduced to a greater extent in regions that developed LV RWMA compared to those that did not.

In conclusion, HD induced a pronounced fall in myocardial perfusion. As myocardial perfusion fell already early during HD without significant UF not only hypovolemia but also acute dialysis-mediated factors seem to play a role. HD-induced reductions in myocardial perfusion may well play a role in the pathogenesis of HD-related adverse cardiac events.

2.1.3 Ischemia as a cause for the progression of heart failure in patients with idiopathic dilated cardiomyopathy and the effect of beta-blocker therapy

In cooperation with Dept. Cardiology, supported by the Dutch Heart Foundation

Chronic heart failure (CHF) is accompanied by metabolic adaptations and abnormalities, which may lead to myocardial ischemia. It has been shown that the combination of increased demand (increased wall stress and heart rate) and decreased supply leads to an “energy mismatch”, which may cause myocardial ischemia. This was shown by a study using positron emission tomography (PET) in patients who have CHF due to idiopathic dilated cardiomyopathy (IDC) in whom myocardial blood flow (MBF) reserve after maximal vasodilation was markedly impaired in proportion to the severity of CHF. A recent study using dobutamine stress testing (DST) employing echocardiography in patients with IDC further supports this, as abnormal contractile responses during DST compatible with myocardial ischemia were observed in 70 % of the patients.

The present study is aimed at a systematic comparison of the above mentioned findings, before and after therapy with a beta blocker (metoprolol). Our hypothesis is that perfusion-metabolism mismatch and “ischemic” responses to inotropic stimulation are parallel findings, which would corroborate the “ischemia hypothesis”. Furthermore we hypothesize that PET mismatch and biphasic response to inotropic stimulation represent a vulnerable situation of the myocardium in patients with IDC, which is, however, accessible to therapy with a beta blocker.

In 30 patients with a new diagnosis of IDC, before starting beta blocker therapy, a ^{13}N-NH_3-PET study with functional parametric mapping is performed to show perfusion at rest and during dipyridamole infusion. Glucose uptake is studied with ^{18}F-FDG-PET. Within one week, a MRI scan is also performed, in which wall thickening is determined in 13 myocardial segments, both at rest and during dobutamine infusion of 5 to 40 µg/kg/min. Thereafter patients are treated with increasing doses of metoprolol, as high as they will tolerate clinically.

We expect to observe a matching of the myocardial segments showing perfusion-metabolism mismatch in PET and an ischemic biphasic response to dobutamine in MRI. Furthermore, we expect to find an improvement of function after beta blocker therapy, particularly in these regions. The study is currently in progress.

2.1.4 Cardiac Assessment of Patients with Late Stage Duchenne Muscular Dystrophy

In cooperation with Dept. Cardiology

Prolonging life expectancy by mechanical ventilation in patients with Duchenne muscular dystrophy (DMD) makes the question for an adequate cardiac evaluation more relevant. Echocardiography has been considered the gold standard until now. We added determinations of N-terminal pro-Brain Natriuretic Peptide (NT-proBNP) in human plasma and multigated cardiac radionuclide ventriculography (MUGA) and investigated the relationship between NT-proBNP, echocardiography and MUGA in DMD.

We studied all adult, ventilation-dependent DMD patients who attended our multidisciplinary outpatient clinic. Echocardiography classified left ventricular (LV) and right ventricular (RV) function as either normal or minor, moderate or severe dysfunction. Plasma NT-proBNP was determined using immunoassay on the same day. LV and RV function and LV ejection fraction (LVEF) were also determined using MUGA.

Data were collected from 18 patients. The mean level of NT-proBNP was 165 ng/l (SD 147). Echocardiography and MUGA showed abnormal LV function in 81 and 64% of the patients, respectively. NT-proBNP levels showed a weak correlation with LV dysfunction on echocardiogram. The NT-proBNP level showed a significant correlation to LVEF and LV dysfunction on MUGA. The concordance rate between echocardiography and MUGA regarding LV function was 73%. Image quality was much more often suboptimal in echocardiograms than in MUGAs: 94% versus 18%.

NT-proBNP levels were not related to age, use of cardiac medication, type or duration of ventilatory support, required minute volume, pulmonary function, oxygen saturation, heart rate, blood pressure, features of heart failure or RV function.

In conclusion, determinations of plasma NT-proBNP can play a role in the screening or follow-up of DMD cardiomyopathy as the levels of this peptide show a significant correlation with echocardiographic and MUGA results in this group of patients.

MUGAs appear technically superior to echocardiograms for the cardiac assessment of DMD patients.

2.1.5 The importance of left ventricular function for long-term outcome after primary percutaneous coronary intervention

In cooperation with Dept. Cardiology (Groningen) and Depts. Cardiology and Nuclear Medicine, Isala Klinieken, Zwolle, The Netherlands

The aim of this study was to determine the long-term prognostic value of global left ventricular function assessed by radionuclide ventriculography after myocardial infarction treated by primary percutaneous coronary intervention (PCI).

In a multicenter registry of primary PCI patients, 925 patients underwent routine planar radionuclide ventriculography with a standard dose of 500 MBq of ^{99m}Tc-pertechnetate at a median of 2 days after myocardial infarction for global left ventricular function analysis. The average time of follow-up was 2.5 years.

Mean age (± SD) was 60 ± 12 years, and left ventricular ejection fraction was 45.7 ± 12.2 %. The one-year survival was 97.3 % and the three-year survival 94.2 %. By univariate analysis, Killip class, multi vessel-disease, previous cardiovascular events, peak creatine kinase and its MB fraction, age and left ventricular ejection fraction proved to be predictors of death. Age and left ventricular ejection fraction were shown to be independent predictors of the 1- and 3-year mortality, using a forward conditional Cox regression model.

In conclusion, global left ventricular function measured as left ventricular ejection fraction by radionuclide ventriculography before discharge from the hospital, after primary percutaneous coronary intervention for ST-elevation myocardial infarction, is a powerful predictor of long term prognosis.

2.1.6 Identification of the role of sympathetic innervation in the modulation of the arrhythmogenic substrate in patients with increased risk of sudden death due to ventricular tachy-arrhythmias in the setting of coronary artery disease. A pilot study

In cooperation with Dept.Cardiology, Isala Clinics, Zwolle, The Netherlands

Patients with coronary artery disease and with cardiac ischemia and severe left ventricular dysfunction are at increased risk to develop ventricular tachy-arrhythmias. Expensive implantable cardioverter defibrillators (ICD) are needed to protect such patients against fatal ventricular arrhythmias. However, most of these patients will never develop fatal arrhythymias. A more accurate method to select patients for ICD implantation is urgently required. Positron Emission Tomography (PET) with ^{11}C-hydroxyephedrine (^{11}C-HED) is an attractive non-invasive method to quantify the activity and distribution of the norepinephrine reuptake transporter which can be used as a measure of sympathetic innervation. ^{11}C-HED PET may become an additional tool to detect patients at risk for ventricular arrhythmias.

Our first aim is to perform a small study to determine ^{11}C-HED uptake and distribution in infarcted and ischemic regions of the left ventricle. Our second aim is to determine whether uptake and distribution of ^{11}C-HED are different in patients at high and low risk for the development of ventricular arrhythmias. This pilot study with 20 patients was initiated by the end of 2006 and was continued in 2007. Thus far, 14 patients have been included. The study is expected to end in 2008.

2.1.7 Identification of the role of sympathetic innervation in heart failure patients treated with cardiac resynchronization therapy. A pilot study

In cooperation with the Thorax Center

This pilot study aims: 1.To assess whether baseline sympathetic innervation in patients with chronic heart failure (CHF) is predictive for their response to cardiac resynchronization therapy (CRT), and 2. To assess whether a positive response to CRT coincides with restoration of regional sympathetic innervation.

Patients with non-ischemic cardiomyopathy and an indication for CRT will be approached to take part in the study. The total number of patients will be limited to 15.

Prior to CRT implantation and after six months of follow-up, patients will undergo a $^{13}NH_3$ and ^{11}C-HED PET scan to determine whether there are any changes in blood flow and sympathetic innervation.

The study has started in the summer of 2007. The six-month period of follow-up will end in the summer of 2008.

2.2 Neuroscience

2.2.1 [^{11}C]-PK11195-PET: a tool to monitor anti-inflammatory treatment in Parkinson's disease?

In cooperation with Dept. Neurology

Activated microglia may contribute to the pathologic process in Parkinson's disease (PD). Microglia activation has been measured *in vivo*, both in animal models and in humans, using [^{11}C]-PK11195 and PET. COX-2 inhibition has been shown to reduce neuroinflammation and neurodegeneration in animal models of PD. Thus, [^{11}C]-PK11195 and PET may be used to assess the effect of COX-2 inhibition in PD.

Ten PD patients and eight healthy, age-matched control subjects underwent both a [^{11}C]-PK11195 PET and an MRI scan. A pilot group of 4 PD patients was scanned before and after one month of treatment with celecoxib (200 mg/day) in order to evaluate the ability of COX-2 inhibition to reduce neuroinflammation in PD.

Arterial plasma sampling and metabolite analysis were performed to acquire metabolite-corrected plasma input curves. Statistical Parametric Mapping (SPM2) was used for co-registration of the MRI to the PET scans and for spatial normalisation to the SPM MRI template. Time activity curves (TACs) were made of selected regions of interest (ROIs). Several methods for kinetic modelling of the [^{11}C]-PK11195 data were applied.

First, the cerebellum was used as a reference region to calculate binding potential values (BP) with a simplified reference tissue model (SRTM). Second, cluster analysis (Gunn et al 1998; software kindly provided by the MRC Clinical Sciences Centre, Imperial College, London, UK) was applied to extract a reference region for SRTM. Third, BP was calculated using K3/K4 derived from a two-tissue compartment model. Finally, Logan analysis was used to calculate distribution volumes (DV).

Using the cluster analysis, PD patients showed higher values for BP in putamen and midbrain than controls, although considerable overlap was seen and the differences were not statistically significant. In all PD cases except one, the highest value for BP in the putamen corresponded not to the most affected side of clinical disease, but to the contralateral side. Many values for BP had to be discarded because of fitting errors. Use of the cerebellum as a reference region gave fewer fitting errors but resulted in lower BP values, especially in the PD group. After celecoxib treatment, similar or even higher BP values were observed, without any change in K1. BP values calculated from K3/K4 were correlated with the SRTM results but the absolute values for BP were 10-fold higher. Logan analysis did not indicate any differences between PD patients and controls.

Accurate analysis of [^{11}C]-PK11195 uptake is hindered by a low specific and a high nonspecific binding of the tracer in the brain, combined with very high levels of radioactivity in the vasculature and in extracranial structures. Our main conclusion is

that the current analysis methods produce highly variable results for [^{11}C]-PK11195 binding, which may explain the conflicting results reported in the literature.

In our study, an increased BP of [^{11}C]-PK11195 was observed after celecoxib treatment, which could be due to an exacerbation of neuroinflammation after COX-2 inhibition, which has also been reported in the literature (Colville-Nash and Gilroy 2001). However, in current practice [^{11}C]-PK11195 seems to be not suitable for accurate measurement of the effects of anti-inflammatory treatment. Refinement of the analysis methods to quantify [^{11}C]-PK11195 uptake and the development of better tracers to measure neuroinflammation *in vivo* is urgently required.

2.2.2 Decreased blood-brain barrier P-glycoprotein function in the progression of Parkinson's disease, PSP and MSA

In cooperation with Depts. Neurology and Psychiatry

A decreased efflux function of the P-glycoprotein (P-gp) transport system in the blood-brain barrier (BBB) could facilitate the accumulation of toxic compounds in the brain and increase the risk of neurodegenerative pathology such as Parkinson's disease (PD).

This study investigated P-gp function in the BBB of patients with Parkinsonian neurodegenerative syndromes, using [^{11}C]-verapamil and PET. Patients with PD, progessive supranuclear palsy (PSP) and multiple system atrophy (MSA) were examined. Regional differences in distribution volume were studied using statistical parametric mapping (SPM). An elevated tracer uptake was interpreted as a reduction of P-gp function.

Patients with advanced PD and PSP showed an increased uptake of [^{11}C]-verapamil in frontal white matter regions as compared to controls; while patients with de novo PD showed a lower uptake in the midbrain and in frontal regions. Patients with PSP and MSA showed increased uptake in the basal ganglia.

A decreased function of P-gp in the BBB seems to be a late event in neurodegenerative disorders, and could enhance continuous neurodegeneration. A reduced uptake of [^{11}C]-verapamil in the midbrain and the frontal regions of de novo PD patients may indicate a regional up-regulation of P-gp function.

2.2.3 Blood-brain barrier P-glycoprotein function decreases in specific brain regions during aging: a possible role in progressive neurodegeneration

In cooperation with Dept. Neurology

Cerebrovascular P-glycoprotein (P-gp) at the blood-brain barrier acts as an active efflux pump which limits the cerebral entry of several endogenous and exogenous compounds. An age-associated decline in P-gp function may cause an increased accumulation of toxic substances within the brain and increase the risk of neurodegenerative pathology with aging. We hypothesized that P-gp function in the

blood-brain barrier of healthy subjects may be regionally reduced during normal ageing.

We studied cerebrovascular P-gp function in seventeen healthy volunteers with ages ranging from 18 to 86 years, using [^{11}C]-verapamil and PET. Logan analysis was used to calculate the distribution volume of [^{11}C]-verapamil in the brain. Statistical Parametric Mapping was used to study regional differences between old and young subjects.

Older subjects showed a significantly reduced P-gp function in internal capsule and corona radiata white matter and in orbitofrontal regions. A decreased P-gp function at the blood-brain barrier in these regions may thus explain part of the vulnerability of the aging brain to white matter degeneration. A decreased P-gp function with aging could also be a risk factor for the development of neurodegenerative disease.

.

2.3 Oncology

2.3.1 Na^{18}F-PET for the detection of bone metastases in prostate cancer

In cooperation with Dept. Urology

Bone metastases are present in up to 20% of the newly diagnosed patients with prostate cancer (PCa), but the incidence rapidly increases in progressive disease and can reach 85-100% in hormone-refractory patients. ^{99m}Tc-labeled diphosphonates and gamma camera bone scanning are normally used to assess the presence of metastases. The positron-emitting radiopharmaceutical ^{18}F-fluoride and PET offer the potential of increased resolution and anatomic precision compared to gamma camera bone scanning. Although some data in the literature are favouring the use of [^{18}F]-NaF PET, no prospective study has been done in a homogenous group of patients at risk for bone metastases.

Patients with histologically proven prostate cancer at risk for bone metastases (PSA ≥ 15 ng/l and Gleason score ≥ 7) were included and underwent a [^{18}F]-NaF PET (PET) scan. Also, whole body ^{99m}TcMDP-bone scintigraphy (BS) and MRI (T1, T2, TIRM) of the spinal column and pelvis were performed. After intravenous administration of 200 MBq [^{18}F]-NaF, a PET scan was made using a Siemens ECAT HR+ camera. An iterative reconstruction algorithm (OSEM) was applied. Images were corrected for attenuation. The results of the [^{18}F]-NaF PET scan were compared with those of the MDP and the MRI scans, using the latter as the gold standard. PET and planar bone scans were read independently by 2 experienced nuclear medicine specialists, who were blinded for the clinical data. The McNemar test on discordance was used to compare the findings.

38 patients were included; 31 were examined with all 3 imaging modalities. The mean age was 68 years and the median serum PSA was 39.5 ng/mL (range 9-2903 ng/mL). Readability of the [^{18}F]-NaF PET scans was excellent, because of the detailed images. For BS, patient based sensitivity and specificity for the presence of bone metastases was 50% and 83% respectively for reader X and was 46% and 100% respectively for reader Y. For NaF PET, patient based sensitivity and specificity was 58 / 67% for reader X, and 50 / 58% for reader Y. The positive and negative predictive values for the two readers in both [^{18}F]-fluoride PET and ^{99m}TcMDP BS, though not different, were remarkable low over the studied population.

In conclusion, the scintigraphic results with [^{18}F]NaF-PET in PCa patients at high risk for bone metastases are comparable to those acquired with BS.

2.3.2 Value of ^{18}F-L-DOPA-PET in the follow-up of patients with biochemical evidence of medullary thyroid cancer

In cooperation with Depts. Medical Oncology, Clinical Chemistry and Pathology and Laboratory Medicine, supported by the Dutch Cancer Society (grant 2003-2936)

Aim of our study was to assess the value of DOPA PET for the detection of recurrent or residual medullary thyroid cancer (MTC) in patients with elevated calcitonin after surgery in comparison with FDG PET, Tc-V-dimercapto-succinic acid (DMSA) scintigraphy and morphological imaging (CT or MRI).

Patients with histologically proven MTC with increased serum calcitonin or carcinoembryonic antigen (CEA) levels suspected of recurrent disease were included. Whole body DOPA PET was performed after injection of 200 MBq DOPA and oral pretreatment with carbidopa. FDG PET, Tc-V-DMSA scintigraphy, CT or MRI were performed within a short interval. Endpoints were: number of positive patients, positive body regions and positive lesions. Image interpretation of DOPA PET was blinded from other studies. Newly detected lesions were validated using conventional methods when feasible.

24 patients (M:F=10:14) were entered. 12 patients had sporadic MTC, 11 multiple endocrine neoplasia (MEN) syndrome 2A and one MEN 2B. All patients had elevated serum calcitonin levels (median 1064 ng/l) and 68% had abnormal CEA levels (median 11,9µg). DOPA PET was positive in 15/24 patients, FDG PET, Tc-V-DMSA and morphological imaging methods in 3/15, 4/14 and 8/18 respectively. Of 21 patients, all imaging methods together detected 16 positive patients. 14 were detected with DOPA PET (sensitivity 88%) and 10 with the combination of FDG PET, Tc-V-DMSA and morphologic imaging (CI) (67%). All imaging methods together detected 32 positive regions, 28 were with DOPA PET (88%) and 24 with CI (77%). A total of 118 positive lesions was detected, 79 (70%) with DOPA PET and 85 with CI (72%).

In conclusion, ^{18}FDOPA PET is superior to conventional imaging methods for the detection of medullary thyroid tumor on the patient and regional level. On a lesional-based analysis, conventional methods perform equal to ^{18}FDOPA PET.

2.3.3 ^{11}C-5-HTP and ^{18}F-DOPA PET superior for staging carcinoid and islet cell tumors

In cooperation with Depts. Medical Oncology, Clinical Chemistry and Pathology and Laboratory Medicine, supported by the Dutch Cancer Society (grant 2003-2936)

The aim of the study was to assess the value of whole body ^{11}C-5-hydroxytryptophan (HTP) positron emission tomography (PET) versus whole body ^{18}F-fluoro-L-DOPA PET (DOPA) for staging patients with carcinoid and islet cell tumors, in comparison with the generally used gold standard of abdominal CT in combination with whole body somatostatin receptor scintigraphy (SRS).

Whole body PET scans were performed after oral carbidopa with injection of 100-200 MBq ^{11}C-5-HTP and 100 - 200 MBq DOPA in patients with carcinoid or islet cell tumors. CT scanning and SRS were performed within a short interval using standard methods. Endpoints were the number of positive patients, positive body regions and individual lesions. As a gold standard, we used a composite reference standard consisting of all available histological and imaging (CT, SRS) data. Image interpretation of PET was blinded from the other studies. Newly detected lesions on PET were validated using conventional methods when feasible.

In this ongoing study, 30 patients (M:F=16:14) were entered, of which 20 had a carcinoid tumor and 10 an islet cell tumor. In carcinoid tumors, HTP PET was positive in 20 of 20 patients (sensitivity 100%, 11 lesions per patient (lpp)) DOPA PET in 20 of 20 patients (sensitivity 100%, 11lpp), CT in 19 of 20 patients (sensitivity 95%, 8 lpp), SRS in 16 of 20 patients (sensitivity 80%, 7 lpp). In islet cell tumors, HTP PET was positive in 10 of 10 patients (sensitivity 100%, 12 lesions per patient (lpp)) DOPA PET in 7 of 10 patients (sensitivity 70%, 5 lpp), CT in 9 of 10 patients (sensitivity 90%, 10 lpp), SRS in 5 of 10 patients (sensitivity 50%, 5 lpp).

Thus, for staging islet cell tumors, HTP PET was clearly superior to DOPA PET and conventional imaging methods, whereas for carcinoid tumors DOPA PET was slightly better then HTP PET and clearly superior to CT and SRS.

2.3.4 Value of FDG PET for Confirmation of N0 Neck and Detection of Occult Metastases in Oral and Oropharyngeal Cancer

In cooperation with Depts. Maxillofacial Surgery, Otorhinolaryngology, Pathology and Radiology

Treatment of the clinical N0 neck in squamous cell carcinoma (SCC) of the oral cavity and oropharynx remains a dilemma. None of the current imaging modalities is able to detect the presence of micrometastases in the lymph nodes of clinical N0 necks reliably. Aim of this study is to determine the diagnostic properties of fluorine-18 fluorodeoxyglucose positron emission tomography (FDG PET) in patients clinically staged as N0 compared to conventional imaging methods. Additionally, the usefulness of whole-body FDG PET in detecting distant metastases and second primary tumors is analyzed.

FDG PET results of 38 patients were compared to histologic specimens obtained with neck dissections or to follow-up with a minimum of 1.5 years. FDG PET performance was compared to the conventional imaging modalities: Computed Tomography (CT), Magnetic Resonance Imaging (MRI) or Ultrasonography-guided Fine Needle Aspiration Cytology (USgFNAC). Besides staging the neck, the FDG PET whole body scan was also evaluated for the detection of distant metastases or second primary tumors.

Sensitivity and specificity of FDG PET in detecting occult cervical metastases were 50% and 97% respectively. Sensitivity and specificity of conventional imaging

methods were 50% and 70% respectively. Two out of three second primary tumors were detected exclusively by FDG PET.

Although FDG PET performed better than conventional imaging modalities, the sensitivity remains lower than desired. Clinical application of FDG PET in the patient staged as N0 seems to be limited. Because of the low incidence, FDG PET in whole body mode is not suitable when it is used only to detect distant malignancy.

2.4 Miscellaneous

2.4.1 Instant vertebral assessment (IVA) in combination with bone densitometry (BDM): A new standard in the diagnosis of osteoporosis?

In cooperation with Dept. Endocrinology and Dept. Nuclear Medicine, Hamilton Health Services, Hamilton, Ontario, Canada

Prevalent vertebral fractures constitute a significant risk factor for future fractures, which is independent of the bone density. New developments in bone density scan (DEXA) machines allow visual and software-based detection of vertebral fractures. We aimed to determine the added value of IVA performed immediately after BDM.

All patients referred to our university medical center department for BDM also underwent IVA om a Hologic Discovery A bone densitometer. Studies were analyzed by 3 experienced operators and physicians. The frequency of vertebral fractures was determined in the entire cohort and in various subgroups. Referring physicians were asked for their opinion on the added value of IVA using a short questionnaire.

958 patients were included (64% females, 52% postmenopausal), 29% were assessed because of primary osteoporosis, 71% for secondary osteoporosis. 30% used corticosteroids. In 2%, IVA was not possible due to extreme adipositas or deformities. In 71%, T4 and in 86%, T5 was the upper vertebral level that could be assessed. The main finding in this cohort was a prevalence of vertebral fractures of 26%. In 68% of these patients, this fracture was previously unknown. We found a mean of 1.8 vertebral fractures per patient. Even after excluding mild fractures (=20-25% height loss) still 17% of the patients had moderate (>25%) or severe (>40% height loss) vertebral fractures. In the 27% with normal bone density the vertebral fracture prevalence was still 18%, in the 43% with ostopenia 23%, and in the 29% with osteoporisis 36%. In primary osteoporosis, the vertebral fracture prevalence was 45%, in secondary osteoporosis 33%. Referring physicians reported that in 58% of the cases, IVA results increased their understanding, and in 27% had an impact on treatment.

In conclusion, IVA added to BMD is a very convenient and patient-friendly diagnostic tool with a high diagnostic yield as the method detected vertebral fractures in 1 out of 4 patients. In 2/3 of these cases these fractures were previously unknown. In 18% of the patients with normal bone density, vertebral fractures were detected.

BASIC RESEARCH

3.1 Animal studies

3.1.1 Functional PET imaging: a versatile tool for regulatory studies on developmental neurotoxicity

In cooperation with TNO Quality of Life, Zeist, the Netherlands.

Children and unborn foetuses are daily exposed to chemicals from the environment, medication, drinking water and food. However, many dossiers of regulated substances lack specific data on their effects on the foetus, neonate and juvenile. Safety information from adults does not always adequately predict safety profiles for paediatric groups, especially for immature systems like the developing brain. Nevertheless, existing international guidelines for toxicity testing focus on exposure of adult animals and on physical malformations of the newborn after exposure during pregnancy, but not on functional defects. With regard to developmental neurotoxicity testing, regulatory agencies (Organisation for Economic Co-operation and Development OECD, Environmental Protection Agency EPA) have issued (draft) guidelines focusing on toxicity endpoints not included in any other guideline: i.e. neuropathology (brain structure) and behaviour (brain function). However, behavioural tests show symptoms of developmental neurotoxicity indirectly, not in the brain itself, whereas the neuropathology endpoints, such as conventional microscopic slide reading, are not very sensitive (De Groot DMG et al., *Envir.Toxicol.Pharmacol*., 19:745-755, 2005). Advanced stereology is sensitive and has high discriminative power, but it is also laborious and time consuming. Since several animals have to be sacrificed at each test-age, developmental neurotoxicity studies require the sacrifice of many laboratory animals. As an alternative approach, we investigated the potential of functional imaging with [^{18}F]FDG PET for assessment of developmental neurotoxicity.

In a pilot study, female rats were exposed to the proliferation inhibitor methyl-azoxymethanol (MAM, 7.5 mg/kg/d) during day 13-15 of pregnancy. Cerebral [^{18}F]FDG uptake (representing brain activity) was repetitively and non-invasively monitored by microPET from postnatal day 18 to 61. To this purpose, pups were intraperitoneally injected with approximately 20 MBq [^{18}F]FDG and subsequently placed in a black wooden box in a dark room with monotonous background noise. After 50 min, animals were anesthetised with isoflurane gas and placed in the microPET scanner. A 20 min emission scan, followed by a 5 min transmission scan were performed. PET data were reconstructed, co-registered to an age-dependent FDG template and analysed by ROI analysis. In parallel experiments, the motor activity of the offspring (n=10) was measured according to the current developmental neurotoxicity guidelines (US Environmental Protection Agency, Office of Prevention, Pesticides and Toxic Substances 6800/6300; Organisation for Economic Co-operation and Development 426, draft).

The time course of motor activity development of animals in the treatment group differed from that of controls: motor activity of the MAM group was initially lower at

postnatal day 13, but exceeded that of controls on days 21 and 60. However, differences between groups never reached significance due to large inter-individual variations among animals. In contrast, regional cerebral [^{18}F]FDG uptake in the MAM-treated group was significantly lower than in the control group at day 18 (24-32%, depending on the specific brain region; t-test, $p<0.05$, see Fig.1). This difference in [^{18}F]FDG uptake was gradually reduced over time, with a residual discrepancy of only 10% at day 61 (p=NS). Between day 18 and 35, [^{18}F]FDG uptake was significantly increased in frontal cortex, striatum and thalamus in the MAM-treated group (by 18-28% with respect to the day 18 value), whereas no significant changes in FDG uptake were observed in the control group at all (<10%). Between day 35 and 61, [^{18}F]FDG uptake was significantly increased only in the frontal cortex in both groups.

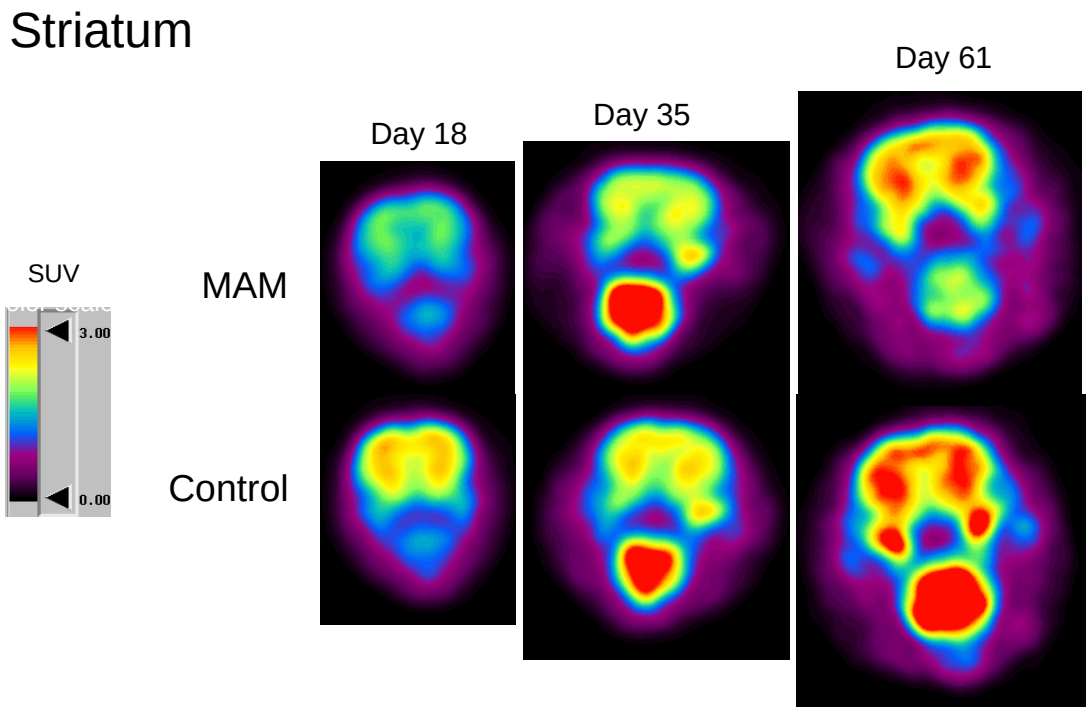

Figure 1. Brain uptake of ^{18}F-FDG in awake young rats which had been prenatally exposed to methylazoxymethanol (upper row of images) or saline (bottom row). Transaxial images of the brain at the level of the striatum are presented. Note the reduction of FDG uptake in the animal treated with MAM as compared to the control.

Repeated motor activity assessment is proposed in current developmental neurotoxicity test guidelines, but it is an apical test that addresses not only locomotion, but also e.g. habituation, arousal and anxiety. Apart from that, indirect effects on locomotion resulting from e.g. differences in body weight and temperature that are not directly related to impaired nervous system development may be detected as well and may lead to false conclusions. So, the design and relevance of tests for developmental neurotoxicity testing is still a matter of debate. In this pilot study, we demonstrated that first generation neurotoxic and developmental effects of MAM can be detected by FDG PET, even when only few animals are used. The observed effects correspond to the mechanism of action of MAM, since the frontal cortex of the fetal brain was in the proliferation phase of development at the time the drug was dosed

(day 13 to 15 of pregnancy). The observed changes in cerebral [^{18}F]FDG uptake over time were also in line with the observed changes in motor activity in the offspring, but PET appears to have superior sensitivity to detect the deficits. Taken together, these observations warrant further evaluation of a potential role of functional imaging techniques in guidelines for developmental neurotoxicity studies.

3.1.2 Neurosteroid depletion and suppletion affects binding of the sigma ligand ^{11}C-SA4503 in tumor cells and tumor-bearing rats

In cooperation with Tokyo Metropolitan Institute of Gerontology, Japan

Sigma receptors are implied in disorders of memory and cognition, drug addiction, depression and schizophrenia. These binding sites are strongly over-expressed in many tumors. Neuroactive steroids may be endogenous ligands. We examined changes of binding of the ligand ^{11}C-SA4503 in C6 cells and in living rats after steroid depletion and suppletion.

^{11}C-SA4503 binding was assessed in C6 monolayers by gamma counting and in pentobarbital-anesthetized rats by microPET scanning. C6 cells were either repeatedly washed and incubated in steroid-free medium or exposed to exogenous steroid (1 h or 5 min before tracer addition, respectively). Tumor-bearing male rats were either depleted from neurosteroids by repeated treatment with pentobarbital or injected with progesterone.

Binding of ^{11}C-SA4503 to C6 cells was increased (by about 50%) upon removal and decreased (up to 70%) upon addition of neurosteroid (rank order of potency: progesterone > allopregnanolone = testosterone = androstanolone > DHEA-sulfate, K_d progesterone 33 nM). Steroid depletion increased the SUV-PET of ^{11}C-SA4503 in rodent brain (27%) and tumor (16%) whereas blood pool radioactivity (AUC) was unaffected. Intraperitoneally administered progesterone reduced only tumor SUV and tumor/muscle contrast (36%).

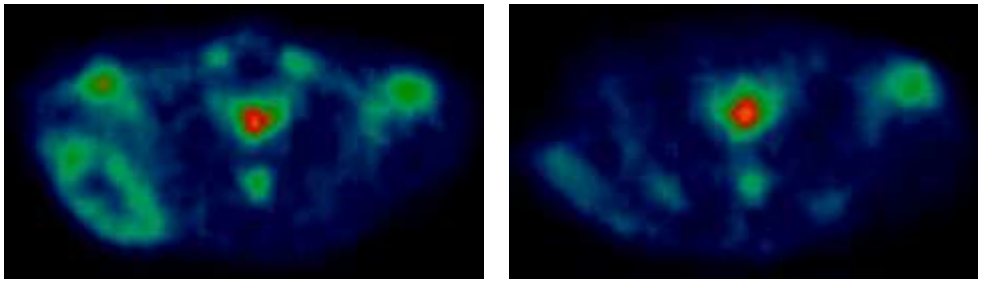

Figure 2. Transaxial ^{11}C-SA4503 images of an untreated tumor-bearing rat (left panel) and a tumor-bearing animal treated with repeated injections of progesterone (right panel). The tumor is located in the lower left corner of each image. Note the significant reduction of tumor-background contrast after progesterone treatment.

In conclusion, cellular binding of ^{11}C-SA4503 is sensitive to neurosteroid competition. Brain uptake of the tracer appears to be particularly sensitive to steroid depletion whereas tumor uptake is affected more by steroid suppletion. Baseline occupancy of sigma receptors by neurosteroids seems to be higher in brain than in periphery.

3.1.3 Radiolabeled COX-2 inhibitors as probes for PET imaging

Cyclooxygenase-2 (COX-2), a key enzyme in the biosynthesis of prostaglandins, plays an important role in neuroinflammation and neuroprotection. COX-2 is overexpressed in affected brain areas in many neurodegenerative diseases. In several neurodegenerative diseases, COX-2 inhibitors were found to have a prophylactic effect.

We have labeled the selective COX-2 inhibitors Celecoxib (CEL) and Rofecoxib (ROF) with carbon-11 and evaluated their utility as PET tracers for COX-2 in healthy rats and in a rat model of herpes simplex encephalitis (HSE) using microPET and ex vivo biodistribution.

In healthy rats, brain uptake of [^{11}C]CEL (SUV 0.9–1.1) was higher than that of [^{11}C]ROF (SUV 0.2–0.4). However, [^{11}C]CEL brain uptake was homogeneous, whereas [^{11}C]ROF distribution did correspond to the known COX-2 distribution. Upon treatment with the COX-2 inhibitor NS398, [^{11}C]ROF uptake was significantly reduced in some brain regions. In HSE rats, [^{11}C]ROF brain uptake appeared to be higher than in healthy controls, but this increase was not statistically significant. [^{11}C]ROF uptake did not correspond to microglia activation, as determined by [^{11}C]PK11195 PET.

Thus, [^{11}C]CEL and [^{11}C]ROF appear not sensitive enough to monitor COX-2 expression with PET, probably due to high non-specific binding.

3.1.4 [^{11}C]Rofecoxib as PET tracer for COX-2: evaluation in a HSV encephalitis model

Cyclooxygenase-2 (COX-2), a key enzyme in prostaglandin biosynthesis, is induced during inflammation. Overexpression of COX-2 is thought to have a detrimental effect in disorders like inflammation, neurodegeneration and cancer. In our previous work, we have evaluated [^{11}C]rofecoxib as a PET tracer for COX-2. Although brain uptake of [^{11}C]rofecoxib in healthy rats corresponded with COX-2 distribution and some specific binding (20-40% of total uptake) was observed, the results were inconclusive, because of the low basal expression of COX-2. In this study, we investigated if inflammation-induced COX-2 overexpression in viral encephalitis could be detected with [^{11}C]rofecoxib PET.

At day 0, viral encephalitis was induced in male Wistar rats by intranasal application of 107 plaque-forming units (PFU) herpes simplex virus type 1 in 100 µl of phosphate-buffered saline (PBS, n=5). Controls were treated identically using PBS

without virus (n=7). After intranasal infection, the replicating virus migrates into the brain where it induces substantial inflammation that causes visible symptoms of illness from day 5 on. At day 6 or 7, the rats were anaesthetized and i.v. injected with 544 MBq [^{11}C]rofecoxib. A dynamic PET scan (microPET Focus 220) was acquired for 60 min, followed by ex vivo biodistribution. In blocking experiments, the non-selective COX inhibitor indomethacin (2.5 mg/kg) was i.v. injected, 5 min before injection of the tracer (n=4).

For all experimental groups, [^{11}C]rofecoxib PET images of the brain showed low tracer uptake at 60 min with minor regional differences. After the initial distribution phase, clearance of the tracer from the brain was slow ($T_{1/2}$ >60 min). Ex vivo biodistribution in healthy controls showed highest [^{11}C]rofecoxib brain uptake in structures with highest basal COX-2 expression: cingular/frontopolar cortex (SUV 0.35 ± 0.11) and hippocampus (SUV 0.30 ± 0.11). Compared to healthy controls, infected animals appeared to show a moderate increase in tracer uptake in all brain regions, but this increase was not statistically significant for any region ($p > 0.14$). The increase in [^{11}C]rofecoxib uptake did not correspond with the distribution of microglia activation, as was determined by [^{11}C]PK11195 PET in a parallel study. At 60 min, radioactivity in plasma was significantly higher in infected animals than in controls (SUV 0.54 ± 0.20 vs. 0.83 ± 0.14, $p = 0.02$), which could explain the elevated brain uptake. Administration of indomethacin to the infected animals did not significantly reduce [^{11}C]rofecoxib uptake in any of the brain regions or in plasma.

In conclusion, [^{11}C]Rofecoxib can not detect neuroinflammation in our viral encephalitis model and therefore it is not a suitable PET tracer for imaging of COX-2 expression in the brain.

3.1.5 PET as a tool for monitoring radiation-induced inflammation and radiosensitation

In cooperation with Dept.Radiotherapy

Primary and metastatic brain tumors are often treated with cranial irradiation. Common complications that occur as a consequence of irradiation can be divided in acute, early-delayed and late effects. The late effects usually appear 3 months after completion of radiation therapy and are most likely to be seen in the subgroup of patients that have a life-expectancy of 5-15 years. These late effects are mainly irreversible and can cause major morbidity.

An important mediator of late complications after cranial irradiation is radiation-induced inflammation. Inflammation of the brain in irradiated patients is accompanied by activation of microglia. The activated glia cells induce a dose-dependent increase in expression of e.g. COX-2, NO-synthase and various cytokines upon irradiation. In neurodegenerative diseases, it was shown that microglia activation precedes neurodegeneration. COX-2 is an important mediator in this process.

Preclinical evidence suggests that COX-2 inhibitors may reduce radiation-induced damage to the brain by preventing the release of prostaglandin E2 and

proinflammatory cytokines. Reduced activation of microglia and astrocytes was also seen after treatment with COX-2 inhibitors. COX-2 inhibitors have other potential benefits as well: they can sensitize brain tumors for radiation therapy and facilitate apoptosis. Interestingly, on the one hand COX-2 inhibitors can sensitize glioblastomas for irradiation, whereas on the other hand the COX-2 inhibitors can reduce radiation damage to normal brain tissue.

Microglia are thought to play a critical role in mediating innate immune responses in case of trauma or infection to the brain. The early detection of microglia activation is necessary for early intervention in different neurodegenerative diseases. Activation of microglia results in increased expression of the peripheral benzodiazepine receptors (PBR). Imaging of activated microglia *in vivo* using positron emission tomography (PET) with ligands targeted to the PBR could be a good approach for diagnosis and monitoring of intervention.

The first aim of this project was to examine the degree of neuroinflammation in the rat brain induced by different irradiation doses, visualized by [^{11}C]-PK11195 PET scans. The [^{11}C]-PK11195 PET scans were made at different time points to get insight in possible changes in microglia activation at different intervals after irradiation. The animal studies showed the following results: rats irradiated with a dose of 5 Gy do not yet show clear microglia activation, whereas in rats irradiated with a dose of 25 Gy a transient activation of microglia can be seen for several days. Increasing the irradiation dose to 50 Gy leads to more obvious and also long-term activation of microglia.

Besides these animal experiments, the effect of radiation on tumor cells and radiosensitation by PK11195 (antagonist of the PBR) and celecoxib (COX-2 inhibitor) were investigated *in vitro*. Glucose metabolism, cell proliferation and PBR expression were evaluated using [^{18}F]-FDG, [^{18}F]-FLT and [^{11}C]-PK11195 respectively. C6 glioma cells were treated with radiosensitizers with or without additional irradiation. Irradiated cells of all groups show increased uptake as compared to non-irradiated cells. Although no significant differences in uptake between non-irradiated and irradiated cells were seen in control and PK11195-treated cells, a trend towards increased [^{18}F]-FDG uptake and thus increased cell metabolism was observed in the irradiated groups. A significant change in relative uptake of [^{18}F]-FDG was seen in celecoxib-treated cells. Irradiated celecoxib-treated cells showed an increased uptake as compared to non-irradiated celecoxib-treated cells. The literature may provide an explanation for this increased uptake of [^{18}F]-FDG, since it is known that celecoxib increases radiation sensitivity in glioblastoma cells. The enhanced sensitivity causes an augmented flare effect and thus an increased [^{18}F]-FDG uptake. Non-irradiated celecoxib-treated cells showed a decreased uptake of [^{18}F]-FDG as compared to the non-irradiated control cells. This may be explained by the fact that celecoxib is cytotoxic and thus causes a reduction of cellular metabolism.

3.1.6 Methionine-PET to quantify radiation-induced damage to normal tissues

In cooperation with Dept.Radiotherapy

For several tumors treated with radiotherapy, escalation of the tumor dose is expected to increase local control. This dose, however, is limited by the dose that the surrounding tissues and organs can tolerate. Therefore detailed knowledge on the relation between the spatial radiation dose distribution in these organs and the risk of (severe) complications would allow further treatment optimization and the probability of complication-free local control.

In head-and-neck cancer patients, dysphagia and xerestomia are frequently occurring side effects, both having a strong impact on the quality of life of the patient. In previous studies we found that the response of the parotid gland to radiation depends on which part of the gland is irradiated (Konings et al., *Int J Radiat Oncol Biol Phys* 2005; 62:1090-1095). While irradiation of the caudal 50% of the gland resulted in loss of 50% of the pre-irradiation function, irradiation of the cranial 50% resulted in losses up to 100%. In the later irradiation, damage was found to extend to the un-irradiated parts of the parotid glands as well (Konings et al., *Int J Radiat Oncol Biol Phys* 2006; 64:98-105).

To study these regional effects in the parotid gland in more detail, techniques to measure function locally in the parotid gland tissue are needed. Several studies exist in which [^{11}C-methyl]methionine PET scanning in patients is used for this purpose. To test the feasibility of using this techniques in rats as well, we performed a pilot study to determine whether we could detect local radiation-induced changes in parotid function. To this end we scanned an un-irradiated control animal and an animal that was irradiated to the caudal 50% of the parotid gland.

Figure 3 shows a rendering of a low-signal (body) and high-signal (parotid and submandibular gland tissue) iso-intensity contours for both animals. Due to the close proximity of the submandibular gland to the parotid gland, these organs could not be distinguished. The effect of irradiating the caudal 50% of the parotid gland, however, is clearly visible by the decreased size of in the cranial-caudal direction.

We conclude that radiation-induced changes in the rat parotid gland can be imaged using an [^{11}C-methyl]methionine PET scan. Additional imaging, however, is required to obtain information on the parotid gland and submandibular gland separately.

Figure 3. ^{11}C-Methionine PET scan of a control animal and an animal of which the caudal half of the parotid gland had been irradiated. Right before the microPET scan, the salivary glands of the animals were stimulated with pilocarpine.

3.1.7 PET imaging of PBR in a rat model of HSV encephalitis

In cooperation with Brain and Mind Research Institute, University of Sydney, Campertown, Australia

Neuroinflammation is associated with a variety of neurological diseases. During neuroinflammation the expression of the peripheral benzodiazepine receptor (PBR) is increased, which can be visualised by positron emission tomography (PET) with [^{11}C]PK11195. However, [^{11}C]PK11195 shows low brain uptake and high non-specific binding and may not be sensitive enough to visualize mild inflammation. Recently, [^{11}C]DPA-713 and [^{18}F]DPA-714 were developed as PET tracers for PBR which are potentially more sensitive than [^{11}C]PK11195.

Both [^{11}C]DPA-713 and [^{18}F]DPA-714 were evaluated in a rat model of herpes simplex encephalitis (HSE) and compared to [^{11}C]PK11195.

The uptake of both [^{18}F]DPA-714 and [^{11}C]PK11195 was significantly higher in affected brain areas in HSE rats as compared to the corresponding brain areas in controls. [^{11}C]DPA-713 uptake was not significantly increased. In controls, basal uptake of [^{18}F]DPA-714 was significantly lower than [^{11}C]PK11195 uptake.

Thus, [^{18}F]DPA-714 is a promising new tracer for neuroinflammation, especially because of its better contrast between inflamed and non-inflamed areas.

3.1.8 [^{18}F]DPA-714 as a novel PET tracer for PBR: a comparison with [^{11}C]PK11195 in a rat model of HSV encephalitis

In cooperation with Center for Mental Health, Winschoten, Netherlands and Brain and Mind Research Institute, University of Sydney, Campertown, Australia. Supported by Stanley Medical Research Institute

Many neurological diseases, including Parkinson's disease and herpes simplex encephalitis (HSE), are associated with neuroinflammation. Expression of the peripheral benzodiazepine receptor (PBR) is increased during neuroinflammation and can be visualised by positron emission tomography (PET) with [^{11}C]PK11195. However, [^{11}C]PK11195 shows low brain uptake and high non-specific binding and may not be sensitive enough to visualise mild inflammation. Recently, [^{18}F]DPA-714 was developed as a more sensitive PET tracer than [^{11}C]PK11195. In this study, [^{18}F]DPA-714 was evaluated and compared to [^{11}C]PK11195 in a rat model of HSE.

DPA-714, the 2-fluoroethyl analog of DPA-713, was prepared by reaction of the corresponding tosylate precursor with K^{18}F / kryptofix in acetonitrile at 100 ^{o}C for 10 min. The product was passed through an Alumina N seppak and purified by reversed phase HPLC. The stability of [^{18}F]DPA-714 was tested ex vivo and in vivo by TLC analysis. Male Wistar rats were intranasally inoculated with the herpes simplex virus type-1 (10^7 PFU in 100 µl PBS) or PBS (control). Within a week after inoculation, replicating virus migrated into the brain and induced neuroinflammation. At day 6 or 7 following inoculation, the rats received an i.v. injection of [^{18}F]DPA-714 (55 ± 9 MBq) or [^{11}C]PK11195 (78 ± 22 MBq) and dynamic PET scans (MicroPET Focus 220) were performed for 2 h and 1 h respectively, followed by ex vivo biodistribution.

[^{18}F]DPA-714 was obtained in 20 ± 5% radiochemical yield, with a specific activity of 104 ± 28 MBq/nmol and a radiochemical purity >99%. Ex vivo, [^{18}F]DPA-714 was stable in rat plasma: 95 ± 1% unchanged [^{18}F]DPA-714 after 2 h at 37 ^{o}C. In vivo, [^{18}F]DPA-714 was converted into more polar metabolites, with 78 ± 1% of the radioactivity in rat plasma consisting of the parent compound 2 h after tracer injection. The PET images of [^{18}F]DPA-714 showed a low tracer uptake in control rats (n=3), which was significantly lower than [^{11}C]PK11195 uptake (n=5) at 1 h ($p=0.01$), and a slow tracer clearance from the brain ($T_{1/2} > 100$ min). [^{18}F]DPA-714 uptake in HSE rats (n=3) was significantly increased (90-150%) in olfactory and retrograde brain areas where HSV-1 accumulates, whereas [^{11}C]PK11195 uptake (n=5) was not significantly increased in these areas.

In conclusion, [^{18}F]DPA-714 is a promising tracer for visualisation of neuroinflammation and is more sensitive than [^{11}C]PK11195 because of a better target-to-nontarget contrast

3.1.9 PET imaging of herpes simplex encephalitis in rats

In cooperation with Center for Mental Health, Winschoten, Netherlands. Supported by Stanley Medical Research Institute.

Approximately 80% of the human population is latently infected with the herpes simplex virus type-1 (HSV-1). HSV-1 is implicated in the etiology of neurological diseases like schizophrenia and Alzheimers disease. In rodents, intranasal inoculation with HSV-1 results in mainly retrograde transneural transport of HSV-1 into the central nervous sytem (CNS), causing the activation of microglia. We used positron emission tomography (PET) to study active HSV-1 in the CNS ([^{18}F]FHBG) and the related microglia activation ([^{11}C]PK11195) in a rat model of herpes simplex encephalitis (HSE). In addition, [^{18}F]FDG was used to study the effect of herpes simplex encephalitis on CNS metabolism.

Male Wistar rats were intranasally inoculated with HSV-1 (10^7 plaque-forming-units in 100 µl phosphate-buffered saline, PBS) or PBS (control). Within a week after the inoculation, replicating virus migrated into the CNS and induced microglia activation. At day 6 or 7 following inoculation the rats received an i.v. injection of [^{18}F]FHBG (22 ± 9 MBq), [^{11}C]PK11195 (78 ± 22 MBq) or [^{18}F]FDG (29 ± 3 MBq). A dynamic PET scan (MicroPET Focus 220) was performed for 60 min, followed by ex vivo biodistribution.

At 60 min the uptake of [^{18}F]FHBG (SUV) in HSE rats (n=8) was significantly higher (200-400%, $p<0.05$) in the bulbus olfactorius, anterior cingulate, frontal cortex and the parietal cortex as compared to controls (n=6). This is consistent with retrograde transneural transport of HSV-1 via olfactory epithelium into the CNS. However, there was a trend towards a higher uptake in all other areas. Microglia activation was found predominately in the brainstem and cerebellum, were the uptake of [^{11}C]PK11195 at 60 min was significantly higher (77% and 158%, $p<0.05$) in HSE rats (n=5) than in controls (n=5). Microglia activation in the brainstem, anterograde to the trigeminal nerve, could be the result of HSV-1 invading the trigeminal nerve, where it is known to establish latency. [^{18}F]FDG showed a global increase in CNS metabolism, with a significantly higher ($p<0.05$) uptake (71 ± 24%) in all brain areas of HSV-1 infected rats (n=8) as compared to controls (n=4). It was an unexpected finding that focal HSV-1 infection caused distant microglia activation and global hypermetabolism.

The combination of [^{18}F]FHBG, [^{11}C]PK11195 and [^{18}F]FDG PET gave an unique insight in the special relationship between HSV-1 infection and specific foci of microglia activation with global hypermetabolism. This may provide a tool for better understanding of the role of HSV-1 infections in debilitating neurological diseases.

3.1.10 Visualization of neuro-inflammation and glucose metabolism with microPET in rats after treatment with methotrexate

In cooperation with Dept. Behavioral Physiology, Groningen University and Dept. Psychosocial Research and Epidemiology, Netherlands Cancer Institute, Amsterdam

Methotrexate (MTX) is a cytostatic agent used in adjuvant chemotherapy for treatment of cancer. Although there is no doubt that chemotherapy increases the survival rate after diagnosis of cancer, it may affect the quality of life up to years after treatment, due to severe side effects. One of the long term effects is cognitive impairment, mostly affecting attention/concentration, speed of information processing and memory. The aim of this study is to examine changes in the brain after treatment with MTX. Therefore, male Wistar rats were treated with 250 mg/kg MTX or saline through the tail vein. One week and 3 weeks after treatment, the animals were placed in a micro PET scanner and examined with two different tracers.

The first experiment examined the effect of MTX on neuro-inflammation, by injection animals with ^{11}C-PK11195. The tracer was injected through the penile vein of anesthetized animals. Thirty minutes later, the animal underwent a static emission scan of 30 minutes, followed by a transmission scan. The second experiment examined the effect of MTX on glucose metabolism, by injection of animals with ^{18}F-FDG. The tracer was injected intraperitoneally; 25 minutes after FDG injection, the animals were anesthetized and placed in the camera for a transmission scan. Forty-five minutes after FDG injection, a static emission scan of 30 minutes duration was made.

The scan data were analyzed with ASIPro and a region of interest (ROI) was drawn around the entire hippocampal area. The standard uptake value (SUV) was calculated with the formula: SUV = [Bq/g tissue in ROI]/[Injected radioactivity in Bq/Body weight in g].

A trend was observed: animals treated with MTX showed a higher uptake of ^{11}C-PK11195 (i.e., more neuroinflammation) and a smaller FDG uptake (i.e., less glucose metabolism) one week after treatment, but this observation failed to reach significance. Three weeks after treatment, the trend was no longer observed, suggesting that any negative effects of MTX are transient.

3.1.11 Neuroinflammation and blood-brain barrier P-glycoprotein function studied with animal-PET in a Parkinson's disease model.

In cooperation with Dept.Neurology

The cause of Parkinson's disease (PD) is so far unknown. Blood brain barrier (BBB) dysfunction and neuroinflammation are thought to play a role in the progression of neurodegeneration. Microglia activation has been measured *in vivo* in animal models and in humans using [^{11}C]-PK11195 PET. Anti-inflammatory treatments have been shown to reduce neuroinflammation and neurodegeneration in animal PD models. [^{11}C]-PK11195 PET could allow quantification of drug effects.

Furthermore, neuroinflammation may influence function of the P-glycoprotein efflux pump in the BBB. Changes in P-gp function have also been detected in PD patients in a study using [^{11}C]-verapamil PET.

Intrastriatal injection of 6-hydroxydopamine (6-OHDA) in rats causes slow and progressive degeneration of the dopaminergic system, by retrograde degeneration of dopaminergic neurons in the substantia nigra. This model has been used extensively as a PD model to study dopaminergic degeneration and has also been used in several studies on neuroinflammation.

We studied neuroinflammation and BBB P-gp function in the 6-OHDA animal PD model, using [^{11}C]-PK11195 and [^{11}C]-verapamil with high resolution animal-PET and post mortem histology for microglia activation, P-gp expression and dopaminergic degeneration. Furthermore, we studied the ability of [^{11}C]-PK11195 and animal-PET to monitor the effect of anti-inflammatory treatment with celecoxib, a COX-2 inhibitor.

We have now scanned four groups of six rats and compared neuroinflammation under 4 conditions: after one week with (i) SHAM-lesion or (ii) 6-OHDA lesion and after three weeks with 6-OHDA lesion (iii) with or (iv) without treatment with celecoxib. Data analysis of this study is in progress.

3.1.12 Effects of chronic stress on blood-brain-barrier function and P-glycoprotein activity

In cooperation with Depts. Molecular Neurobiology and Psychiatry

Chronic and uncontrollable stress is generally considered as an important factor in the development of various diseases, including depression. In this study we apply an animal model of chronic stress to examine effects of stress on P-glycoprotein (P-gp) activity in the brain. P-gp is an efflux pump in the membrane of endothelial cells that plays an important role in blood-brain-barrier function by pumping toxic substances out of the brain back into the bloodstream. Alterations in this protective mechanism may have consequences for brain functioning and could be involved in the pathophysiology of brain diseases like depression. Rats are subjected to a daily session of uncontrollable footshock stress for a period of 3 weeks. This stress protocol is thought to result in persistent changes in physiology and brain function

that may be relevant for our understanding of psychopathologies. At the end of the 3-week stress period, P-gp activity is measured by small animal PET. Rats are subjected to a 1-hour PET scan session after injection of the tracer [^{11}C] verapamil, which is a substrate for P-gp. Brains are collected for Western Blot analysis and/or immuhistochemical analysis of cerebrovascular markers and potential P-gp regulators. Preliminary PET data suggest that chronic stress may decrease P-gp activity. Further measurements and analysis are currently performed to confirm this finding.

3.1.13 Manipulation of [^{11}C]HTP and [^{18}F]FDOPA accumulation in neuroendocrine tumors and tumor cells

In cooperation with Dept.Medical Oncology, Groningen and Dept.Pharmacy, Ghent, Belgium

PET studies for imaging of neuroendocrine tumors (NETs) have recently raised interest. NETs possess the unique property of synthesis, storage and secretion of biogenic amines. Clinically applied tracers to visualize this property are [^{18}F]FDOPA and [^{11}C]-5-hydroxytryptophan ([^{11}C]HTP). Despite the clinical utility of these tracers, little is known about the precise mechanisms that govern their accumulation in tumor cells. The aim of the present study was the analysis of the uptake of [^{11}C]HTP and [^{18}F]FDOPA by large amino acid transporters (LAT), peripheral decarboxylation by amino acid decarboxylase (AADC) and intracellular breakdown by monoamine oxidase (MAO) both *in vitro* and *in vivo*.

Inhibition experiments. Various concentrations of the blocking agent BCH (0-20 mM) were applied to determine an adequate LAT blocking concentration with incubation time of 15 min. Tracer incubation times ranged from 5 to 60 minutes with the AADC inhibitor carbidopa and MAO inhibitors, clorgyline and pargyline. Metabolites resulting from these enzymes (5-HT and 5-HIAA) were analyzed. *MicroPET scanning*. 60 minutes dynamic scanning followed by 10 minutes transmission scanning was performed using a microPET Focus 220 system. Prior to injection of [^{11}C]HTP or [^{18}F]FDOPA, mice from each group received either saline or carbidopa (1 mg/kg) intraperitoneally (IP).

Time-course of tracer accumulation. Both tracers showed very rapid and high accumulation. [^{18}F]FDOPA was accumulated to 1.2±0.2 % / 10^5 cells after 15 minutes and remained constant up to the end of the 60 minutes incubation period. [^{11}C]HTP accumulation was much higher than [^{18}F]FDOPA (ratio 5:1) with a maximum tracer accumulation of 5.3±0.8 % / 10^5 cells at 60 minutes.

Inhibition experiments. The BCH IC_{50} value for [^{11}C]HTP was determined to be 0.12 mM. whereas the BCH IC_{50} value for [^{18}F]FDOPA was 0.01 mM. Incubation of cells with carbidopa did not affect accumulation of both [^{11}C]HTP and [^{18}F]FDOPA. Clorgyline preincubation led to significantly higher accumulation compared to control for [^{11}C]HTP (14.2±3.8 % / 10^5 cells) and [^{18}F]FDOPA (9.2±2.9 % / 10^5 cells) . With pargyline slightly higher accumulation compared to control was obtained for [^{18}F]FDOPA (3.7±0.7 % / 10^5 cells after 60 minutes). Metabolite analysis showed that only low cellular levels of 5-HT (0.6±0.1 %) were found compared to the levels

of 5-HTP (12.0±0.0 %) and of 5-HIAA (11.9±0.8 %). Treatment with carbidopa did neither increase 5-HTP nor decrease cellular levels of 5-HT or 5-HIAA. Clorgyline however increased 5-HT (18.4±2.9 %) and decreased 5-HIAA levels (0.9±0.0 %). Similar results were obtained after pargyline treatment. *Animal experiments* In 33 of 36 mice, tumors were visualized. Treatment with carbidopa resulted in higher SUVs for tumors compared to controls for both tracers within 60 minutes time. [^{18}F]FDOPA generated significantly higher tumor SUVs than [^{11}C]HTP.

Carbidopa did not influence accumulation of both tracers in tumor cells *in vitro* but did increase tumor accumulation of radioactivity in animals *in vivo*. Örlefors *et al.* reported in patients an improved uptake of [^{11}C]HTP in carcinoid tumors after oral administration of carbidopa. This was suggested to be the result of decreased conversion of [^{11}C]HTP and [^{18}F]FDOPA to [^{11}C]5-HT/[^{18}F]dopamine in peripheral tissues, therefore increasing the availability of [^{11}C]HTP. Our results validate this hypothesis. Carbidopa did not affect the accumulation of [^{11}C]HTP or [^{18}F]FDOPA in BON cells. This suggests that intracellular decarboxylation in BON cells was not inhibited.

In vitro, selective inhibition of MAO A by clorgyline induced increased accumulation of both tracers, confirming that the activity of monoamine oxidase is an important factor affecting their biodistribution. [^{11}C]HTP was accumulated twice as much as [^{18}F]FDOPA over a period of 60 minutes. This could be a consequence of the fact that BON cells produce more 5-HT than dopamine. Degradation of [^{18}F]fluorodopamine and [^{11}C]5-HT appears to be blocked by clorgyline. Pargyline gives a slightly higher [^{18}F]FDOPA accumulation compared to control in accordance with the fact that pargyline is also an inhibitor for MAO B. Use of the MAO A inhibitor clorgyline and non-selective MAO inhibitor pargyline resulted in higher intracellular tumor 5-HT and lower 5-HIAA level. Once 5-HT is formed inside the cell, it appears not to be transported outside the cell before being deaminated by MAO to 5-HIAA. Higher concentrations of pargyline could probably also lead to an increased [^{11}C]HTP accumulation.

Retention of [^{11}C]HTP and [^{18}F]FDOPA is considered to be the result of LAT, decarboxylation and granular storage.

3.1.14 Characterization of ^{89}Zr-trastuzumab for clinical HER2 immunoPET imaging

In cooperation with Depts. Medical Oncology and Pharmacy

SPECT imaging with ^{111}In-DTPA-trastuzumab has recently identified new tumor lesions, undetected with conventional staging, in 13/15 patients with HER2++ breast cancers (Perik *et al.*, J Clin Oncol 2006). The aim of this study was to develop an immunoPET label, suitable for clinical use, which would allow excellent detection of HER2 positive tumor lesions and quantification of HER2 expression levels in vivo.

Trastuzumab was radiolabeled as described by Verel *et al.* (*J Nucl Med* 2003). Radiochemical purity (rcp) and stability were determined by SEC-HPLC, immunoreactivity with a Lindmo assay.

Biodistribution was performed in nude mice bearing HER2 positive (SKOV3) or HER2 negative (GLC4) xenografts. Five animals per group were co-injected with ^{111}In-ITC-DTPA-trastuzumab and ^{89}Zr-trastuzumab, imaged on a microPET (Focus 220) and sacrificed 144 hours post injection.

The immunoreactive fraction of ^{89}Zr-trastuzumab was 0.96, labeling efficiency > 90% and rcp > 95%. ^{89}Zr-trastuzumab was stable for 7 days in buffer at 4 °C and in human serum at 37 °C. MicroPET imaging showed excellent tumor uptake and could easily detect metastases with a size approximating the spatial resolution of the microPET scanner. ^{89}Zr- and ^{111}In-ITC-DTPA-trastuzumab showed similar biodistribution. Highest uptake was found in HER2 positive tumors at 144 hours post injection (40% ID/g tissue for ^{89}Zr-trastuzumab and 47% ID/g for ^{111}In-ITC-DTPA-trastuzumab) compared to 8% ID/g tissue in HER2 negative control tumors. Liver uptake was low (8-12% ID/g tissue). Preliminary results in HER2 positive breast cancer patients show excellent tumor tracer uptake and a resolution unapproachable by ^{111}In-DTPA-trastuzumab.

In conclusion, ^{89}Zr-trastuzumab is stable, shows excellent and specific tumor uptake and is suitable for clinical use. Low nonspecific tracer uptake in the liver allows the detection of abdominal metastases.

3.1.15 *In vivo* VEGF imaging with ^{89}Zr-bevacizumab in a human ovarian tumor xenograft model using MicroPET and MicroCT.

In cooperation with Dept.Medical Oncology

VEGF, released by tumor cells, is an important growth factor in tumor angiogenesis as it induces tumor neovascularization. VEGF leads to paracrine effects and results in abundant presence of VEGF in the tumor micro-environment. Non-invasive measurement of VEGF in the tumor may give insight in the available target for VEGF dependent anti-angiogenic therapy. Bevacizumab is a humanized monoclonal antibody which blocks the biological pathways of VEGF induced tumor angiogenesis by binding to VEGF, most likely in the micro-environment of the tumor. For that reason, we developed radiolabeled bevacizumab for *in vivo* VEGF imaging using the relatively new long-lived PET isotope ^{89}Zr ($t_{1/2}$ 3.27d) allowing high resolution (Micro)PET imaging.

Labeling, stability and in-vitro immunoreactivity studies were performed. Thereafter, nude mice were inoculated with VEGF producing human SKOV-3 ovarian tumor cells. After tumor size reached 7-9 mm in diameter, mice were injected with 100 µg (± 3.5 MBq) of ^{89}Zr-bevacizumab or human ^{89}Zr-IgG. Human IgG served as an aspecific control antibody. MicroPET images, MicroCT images and biodistribution studies were obtained at 24, 72 and 168 h post injection. MicroPET and MicroCT images were fused to calculate uptake of ^{89}Zr-bevacizumab and Zr^{89}-IgG in the micro-environment of the tumor.

^{89}Zr-bevacizumab labeling efficiency was >95%. The tracer was stable > 168 h at 37°C in serum. The immunoreactive fraction determined by ELISA was >0.55.

MicroPET images showed uptake in well perfused organs after 24 h and clear tumor localization after 72 h post injection. Tumor uptake determined by quantification of MicroPET images was higher for ^{89}Zr-bevacizumab 168 h post injection, namely 7.38% ± 2.06 IDcm^{-3} compared to 3.39% ± 1.16 IDcm^{-3} for human ^{89}Zr-IgG (p=0.011). These data were confirmed by ex-vivo biodistribution studies. Uptake in other organs was mainly seen in liver and spleen.

The half-life of the PET isotope ^{89}Zr matches the pharmacokinetic half life of bevacizumab. (Micro)PET imaging permits not only excellent visualization, but also dynamic quantification of ^{89}Zr-bevacizumab in the micro-environment of the tumor. Tumor uptake of ^{89}Zr-bevacizumab was significantly higher compared to control ^{89}Zr-IgG, signifying that ^{89}Zr-bevacizumab could potentially be used to visualize VEGF-levels in the micro-environment of the tumor.

3.1.16 *In vivo* VEGF imaging with an anti-VEGF Fab-fragment in a human ovarian tumor xenograft model using MicroPET and MicroCT

In cooperation with Dept.Medical Oncology. Supported by a grant from the Dutch Cancer Society

VEGF, released by tumor cells, is an important growth factor in tumor angiogenesis as it induces tumor neovascularization. $VEGF_{121}$ is freely soluble whereas splice variants like $VEGF_{165, 189, 206}$ are mainly located in the extra cellular matrix resulting in high concentrations in the tumor micro-environment. Previously, we showed that radiolabeled bevacizumab, an intact humanized IgG, is a new tracer for VEGF imaging. Ranibizumab is a humanized Fab-fragment (48 kDa) with high affinity for all VEGF-A isoforms. Ranibizumab is faster cleared from the circulation compared to bevacizumab. We hypothesize that this characteristic could lead to more rapid imaging after tracer administration and a lower radiation dose for patients compared to radiolabeled bevacizumab. For that reason, we developed ranibizumab labeled with PET isotopes for non-invasive VEGF imaging and compared the distribution pattern of this anti-VEGF Fab-fragment with that of radiolabeled bevacizumab.

Labeling, stability and in-vitro immunoreactivity studies were performed. Thereafter, nude mice were inoculated with VEGF producing human SKOV-3 ovarian tumor cells. After tumor size reached 6-8 mm in diameter, a dose escalation study was performed using 3, 8 and 40 μg of ranibizumab per mouse. Radiolabeled Fab-IgG served as a control. MicroPET-, microCT and ex-vivo biodistribution studies were performed at 1, 3, 6 and 24 hr post injection.

Radiolabeling of ranibizumab with ^{18}F and ^{89}Zr resulted in adequate labeling efficiencies. The tracers were stable > 24 hr at 37°C in serum with preserved immunoreactivity. MicroPET images showed rapid renal clearance with high kidney uptake of the Fab-fragment (>100% ID/g). Kidney uptake could be lowered by a co-injection of lysine. Tumor uptake was already high 6 hr post injection. The highest tumor uptake was seen with a low dose of ranibizumab (3 μg). Tumor uptake was significantly higher for radiolabeled ranibizumab compared to Fab-IgG with a tumor/blood (T/B) ratio of respectively 5.7 ± 0.9 vs 1.9 ± 0.2 (p=0.034) 24 hr post injection, which is higher compared to radiolabeled bevacizumab (T/B ratio 2.9 ± 1.6

at 168 hr). Maximal tumor uptake (%ID/gram) was not affected by the fast clearance, with comparable uptake between ^{89}Zr-ranibizumab (24 hr) and ^{89}Zr-bevacizumab (168 hr), respectively 5.5 ± 1.4 vs 6.8 ± 1.8 %ID/g.

Radiolabeling of an anti-VEGF Fab-fragment with PET isotopes permits high resolution microPET imaging. Due to the fast biodistribution of radiolabeled ranibizumab, images could be made earlier after injection compared to radiolabeled bevacizumab. These results demonstrate that ranibizumab, an anti-VEGF Fab-fragment, could be a new tracer to visualize VEGF-levels for the evaluation of anti-VEGF targeted therapy.

3.1.17 Towards clinical VEGF imaging using the anti-VEGF antibody bevacizumab and Fab-fragment ranibizumab

In cooperation with Dept. Medical Oncology. Supported by a grant from the Dutch Cancer Society.

VEGF, released by tumor cells, is an important growth factor in tumor angiogenesis as it induces tumor neovascularization. $VEGF_{121}$ is freely soluble whereas splice variants such as $VEGF_{165,\ 189,\ 206}$ are mainly located in the extra cellular matrix resulting in high concentrations in the tumor micro-environment. Non-invasive assessment of VEGF-levels in the micro-environment of the tumor could guide in the development and follow up of anti-VEGF targeted therapy. For this aim, we radiolabeled the anti-VEGF monoclonal antibody bevacizumab and the Fab-fragment ranibizumab with both SPECT (^{111}In) and PET (^{89}Zr and ^{18}F) isotopes.

Labeling, stability and in-vitro immunoreactivity studies were performed. Thereafter, nude mice were inoculated with VEGF-producing human SKOV-3 ovarian tumor cells. After tumor size reached 6-8 mm in diameter, microPET and biodistribution studies were performed at multiple time points corresponding to the elimination half-lives of radiolabeled bevacizumab and ranibizumab. A feasibility study in patients with recurrent melanoma and metastatic colon cancer has been started.

Uptake was significantly higher for both SPECT- and PET-tracers compared to radiolabeled control (Fab)-IgG, namely 7.7 ± 2.0 %ID/g and 4.7 ± 1.9 %ID/g for respectively ^{111}In-bevacizumab at 168 h and ^{111}In-ranibizumab at 24 h post injection. MicroPET imaging with ^{89}Zr-labeled bevacizumab and ^{89}Zr- and ^{18}F-ranibizumab showed clear tumor localization respectively 72 and 3 h post injection. In addition, uptake of ^{89}Zr-bevacizumab was furthermore predominantly seen in liver and spleen whereas ^{89}Zr- and ^{18}F-ranibizumab was mainly cleared by kidney. Preliminary results of SPECT imaging using ^{111}In-bevacizumab revealed tumor lesions in both recurrent melanoma and metastatic colon cancer patients.

Radiolabeled bevacizumab and ranibizumab showed to be specific tracers for non-invasive (pre)clinical VEGF imaging, with distinctive pharmacokinetics. Bevacizumab shows the highest tumor uptake whereas ranibizumab allows imaging shorter after injection of the tracer. Both these tracers could potentially guide anti-angiogenic VEGF targeted therapy.

3.1.18 MicroCT scans for the study of guided bone regeneration

In cooperation with Dept of Maxillofacial Surgery

In oral implantology, sufficient bone is necessary at the site of implantation of the oral implant. Techniques applied to treat these bony defects are guided bone regeneration (GBR), bone transplantation and the use of bone substitutes.

GBR can be described as the use of a barrier membrane to provide a space available for new bone formation in a bony defect. Barrier membranes are also applied to cover bone grafts; they would prevent bone graft resorption and enhance graft incorporation. There is a continuing debate about this preventive effect. Furthermore, the standard reference membranes, i.e., collagen and ePTFE in GBR are not ideal.

In the first experiment the effect of a new synthetic degradable barrier membrane, poly-DL-lactide-e-caprolactone, PDLLCL, collagen and ePTFE membranes on graft resorption and incorporation of autologous bone grafts in rats were described using microradiography and micro-CT. A total of 192 male Sprague-Dawley rats were treated. A 4.0 mm diameter bone graft was harvested from the right mandibular angle and transplanted to the left. The three barrier membranes were used to cover the grafts. The controls were left uncovered. Graft resorption at 2, 4 and 12 weeks was evaluated by post-mortem microradiography and micro-CT. Data were analysed using multiple regression analyses. Overall, there were no differences in modeling with resorption between the four groups. The mean graft incorporation was progressive and nearly identical from 2 to 12 weeks in all groups. This demonstrates that the indication of barrier membrane-use, to prevent bone modeling with resorption and to enhance incorporation of autologous onlay bone grafts, is at least disputable.

In the second experiment, the effects of the three different types of membranes on bone formation in mandibular critical size defects in rats were evaluated. In the same group of 192 rats, 0.5 mm defects created during bone graft harvesting were treated with the three membranes. Microradiography and micro-CT were used for measurements.

Four groups (control, PDLLCL, collagen, ePTFE) were evaluated at 3 time intervals (2, 4 and 12 weeks). In the membrane groups the defects were covered; in the control group the defects were left uncovered. Data were analysed using a multiple regression model.

Bone formation was progressive in 12 weeks, when the mandibular defect was covered with a membrane. Although substantial bone healing was observed in defects covered with a PDLLCL membrane, overall, more bone formation was observed underneath the collagen and ePTFE membranes than the PDLLCL membranes. The high variation in the PDLLCL samples at 12 weeks may be caused by the moderate adherence of this membrane to bone compared with collagen. PDLLCL in its current composition is not ready for application in clinical practice, although the barrier membrane allows significantly more bone in-growth than the control group.

3.2 Cell studies

3.2.1 Radiolabeling of neural stem cells for PET- and SPECT-imaging

In cooperation with Dept. Membrane Cell Biology

C17.2 cells are immortalized mouse neural stem cells from neonatal cerebellum. These cells show directed migration to sites of inflammation and homing. In order to visualize their migration in an in vivo tumor inflammation model, we checked which labeling method is the most suitable for microPET and microSPECT imaging.

C17.2 cells were labeled for microPET by adding the glucose analog ^{18}FDG in complete cell culture medium (DMEM) with 4.5 g/l glucose, DMEM with 1 g/l glucose or in phosphate-buffered saline (PBS) with calcium and magnesium. Uptake was measured after one hour. Retention of the tracer was measured after labeling for one hour in DMEM with 1 g/l glucose followed by an incubation of two hours in fresh DMEM with 1g/l glucose with or without the glucose transport inhibitor phloretin. For microSPECT, adherent cells were labeled with ^{99m}TcHMPAO during 30 minutes in PBS with calcium and magnesium. Alternatively, cells in suspension were incubated in ^{99m}TcHMPAO solution for 15 minutes. Retention was measured after two hours incubation in complete cell culture medium.

Labeling efficiency with ^{18}FDG in complete cell culture medium with high glucose was 1.4 ± 0.4 % dose/ 10^6 cells (mean ± SD), 4.1 ± 0.4 % in DMEM with low glucose and 11.9 ± 0.5 % in PBS with calcium and magnesium. Retention of ^{18}FDG in DMEM without phloretin was 62%. In the presence of phloretin label retention was enhanced (50□M phloretin – 70% retention; 100□M phloretin - 80% retention and 200□M phloretin - 86% retention).

Labeling efficiency of cells with ^{99m}TcHMPAO in PBS was 12%, which was increased to 50% by labeling the cells in suspension. Retention of ^{99m}TcHMPAO was 80%. ^{18}FDG labeling of C17.2 cells was most efficient in PBS with calcium and magnesium. The high efflux of the tracer could be partly blocked by the addition of phloretin. ^{99m}TcHMPAO labeling of cells showed satisfying efficiency in ^{99m}TcHMPAO solution.

3.2.2 Cytotoxicity of sigma receptor ligands is associated with major changes of cellular metabolism and complete occupancy of the sigma-2 population

In cooperation with Tokyo Metropolitan Institute of Gerontology, Japan

Tumor cells can be selectively killed by application of sigma ligands, but concentrations of 20 to 100 µM should often be administered. High drug doses may be required because diffusion barriers must be passed in order to reach intracellular sites, but also because the entire sigma receptor population should be occupied in order to induce cell death. We measured receptor occupancies associated with the cytotoxic effect and dose-dependent changes of cellular metabolism in a tumor cell line.

C6 cells (rat glioma) were grown in monolayers and exposed to: (a) (+)-pentazocine (sigma-1 agonist), (b) AC915 (sigma-1 antagonist), (c) rimcazole (sigma-1/2 antagonist), or (d) haloperidol (sigma-1/2 antagonist). Occupancy of sigma receptors by the test drugs was measured by studying their competition with cellular binding of the ligand ^{11}C-SA4503. Metabolic changes were quantified by measuring cellular uptake of: (1) ^{18}F-FDG, (2) ^{18}F-FLT, (3) ^{11}C-choline, or (4) ^{11}C-methionine. Cytotoxicity was assessed by observation of cellular morphology and by cell counting after 24 h.

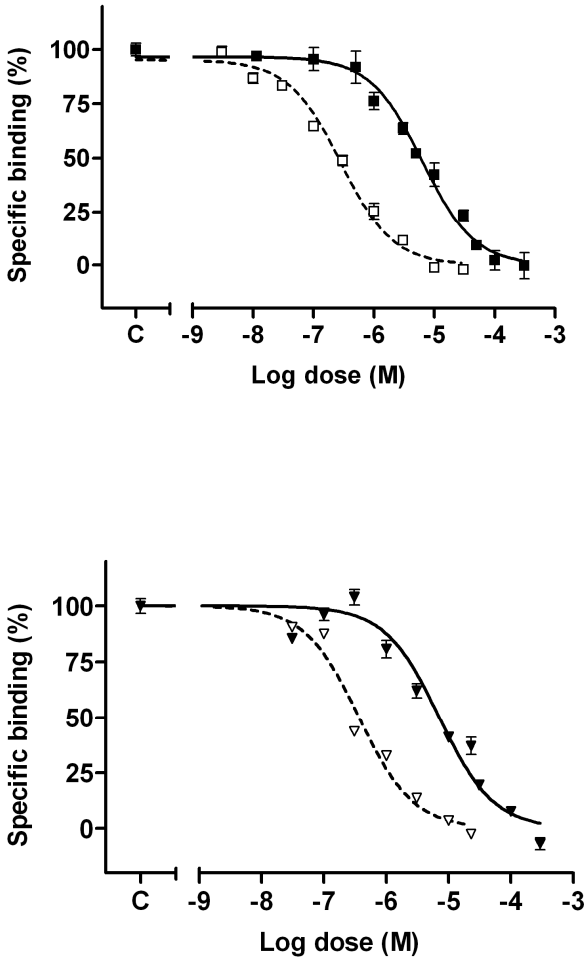

Figure 4.
Dose-dependent inhibition of ^{11}C-SA4503 binding to C6 cells by (+)-pentazocine (solid squares), haloperidol (open squares), AC915 (solid triangles) and rimcazole (open triangles). Error bars indicate s.e.m.

IC_{50} values of the test drugs for inhibition of cellular ^{11}C-SA4503-binding were: 6.5 µM (pentazocine), 7.4 µM (AC915), 0.36 µM (rimcazole) and 0.27 µM (haloperidol), respectively (Fig.4). EC_{50} values (dose required for a 50% reduction of cell number after 24h) were: 710 µM (pentazocine), 819 µM (AC915), 31 µM (rimcazole) and 58 µM (haloperidol), respectively (Fig.5). Cytotoxic doses of sigma ligands were generally associated with increased uptake of FDG, decreased uptake of FLT and choline and little change in methionine uptake per viable cell.

In conclusion, IC_{50} values of the test drugs reflect their in vitro affinities to sigma-2 rather than to sigma-1 receptors. Since cytotoxicity occurred at concentrations two orders of magnitude higher than IC_{50} values for inhibition of cellular ^{11}C-SA4503-binding, loss of cell viability is associated with very high (99%) occupancy of sigma-2 receptors. ^{18}F-FLT, ^{11}C-choline and ^{18}F-FDG responded most strongly to drug treatment and showed changes corresponding to the cytotoxicity of the test compounds.

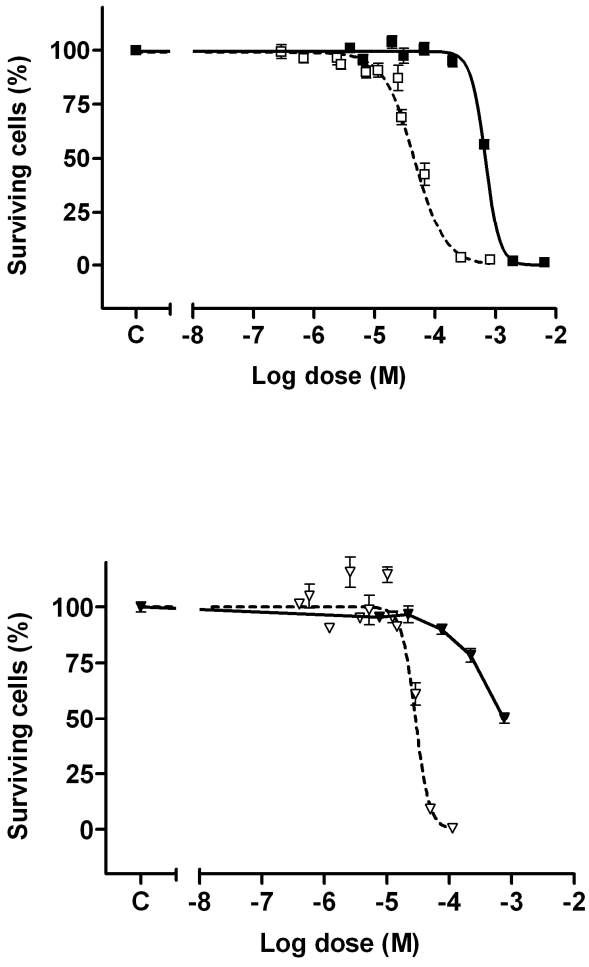

Figure 5.
Dose-dependent killing of C6 cells by (+)-pentazocine (solid squares), haloperidol (open squares), AC915 (solid triangles) and rimcazole (open triangles). Error bars indicate s.e.m.

3.2.3 5-[^{18}F]Fluorotryptophan as a PET tracer for neuroendocrine tumors

In cooperation with Dept.Medical Oncology, Groningen and Dept.Pharmacy, Ghent, Belgium

PET of neuroendocrine tumors (NETs) yields high contrast images using the labeled large amino acids [^{18}F]FDOPA and [^{11}C]-5-hydroxytryptophan ([^{11}C]-5-HTP). While [^{18}F]FDOPA is widely used in imaging NETs, [^{11}C]-5-HTP use is limited to centers with a cyclotron on site due to the short half-life of ^{11}C. Therefore, there is great interest in an ^{18}F labeled tryptophan analog.

To verify if 5-[^{18}F]fluorotryptophan (5-FTP) is a potential PET tracer following the same accumulation mechanism as 5-HTP, we studied non-labeled tracer accumulation in a human neuroendocrine tumor (NET) cell line (BON) with 5-HTP and 5-FTP using AADC and MAO inhibitors.

For the synthesis of [^{18}F]-5-FTP, our strategy was to combine methods used in the synthesis of [^{11}C]HTP and [^{18}F]FDOPA. The synthesis can be divided into two steps (figure), namely first the formation of [^{18}F]fluoroindole, followed by the reversed tryptophanase reaction giving [^{18}F]-5-FTP (Figure 6).

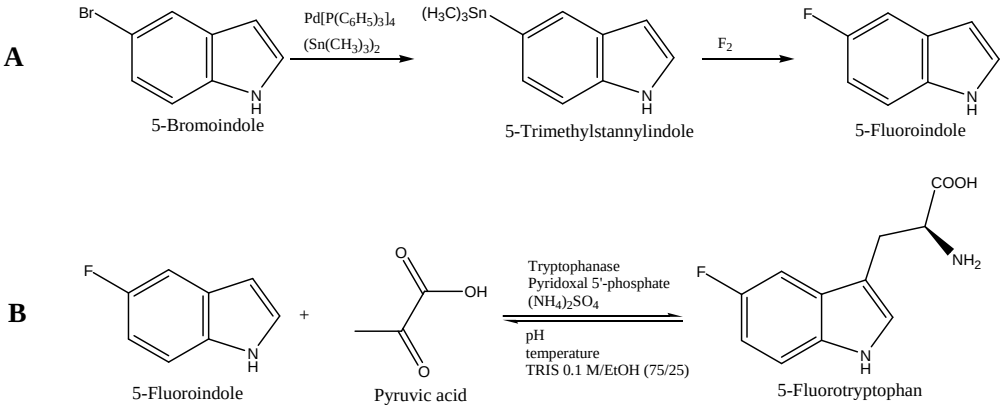

Figure 6. Synthesis of [^{18}F]-5-FTP

The aim of these experiments was to investigate if the enzymatic synthesis of an ^{18}F tryptophan analogue is possible, and if the resulting 5-fluorotryptophan is accumulated in a BON cell line.

For the synthesis of 5-fluoroindole, 71-125 µmol 5-trimethylstannylindole was dissolved in dry acetonitrile and cooled down to 0 °C. 0.3 % F_2 in neon gas was bubbled through the solution within 10 min including one purge of pure neon gas according to an identical procedure for target bombardment. After heating at 50 °C for 10 min in a closed reaction vessel the mixture was filtered via a 22 µm LG filter. The mixture was purified by HPLC. 5-Fluorotryptophan was prepared from purified 5-fluoroindole, which was dissolved in 1.5 ml Tris 0.1 M/ethanol (75/25), 400 µl

ammonium sulfate 1.5 M and 20 µl pyruvic acid. The pH of the mixture was adjusted to 9.5-10. 50 µl tryptophanase and 10 µl pyridoxal 5-phosphate were added and warmed at 40 °C for 10 min. The reaction was stopped by addition of 3 drops of 6M HCl and filtration on a 22 µm GP filter.

Cell experiments were performed in the presence of the AADC inhibitor carbidopa (0.08 mM), the MAO A inhibitor clorgyline (0.1 mM) or the non-selective MAO inhibitor pargyline (0.1 mM). After 15 and 60 min of tracer incubation, buffer was removed. BON cells were harvested with 1 ml trypsin and taken up in 1 ml PBS containing 10% FCS. BON cells were washed three times with ice-cold PBS (1 ml) and centrifuged 10 min at 10,000 g.

Reaction of F_2 gas with 5-trimethylstannylindole gave 15 % yield of 5-fluoroindole. Optimal conditions for the synthesis of 5-FTP using the reversed tryptophanase reaction gave yields of 73 ± 6 %. The reversed tryptophanase reaction was performed on 5-fluoroindole giving 5-FTP confirmed by mass spectroscopy of the collected HPLC peak.

After 15 min of incubation, significant levels of 5-FTP (0.6 % of all 5-FTP in medium) were detected in cell lysates compared to 5-HTP (3.4 % of all 5-HTP in medium). After 60 min incubation period 5-FTP levels remained constant (0.5 % of all 5-FTP in medium) while 5-HTP levels increased over time (12.0 % of all 5-HTP in medium). Treatment with AADC and MAO inhibitors lowered 5-HTP levels after 60 min but led to an increase of 5-FTP levels.

We showed that 5-FTP is taken up into the neuroendocrine pancreatic tumor cell line BON although cellular levels of 5-FTP were lower than 5-HTP levels. Exposure of BON cells to specific AADC and MAO inhibitors led to an increase of cellular 5-FTP. From these data it can be concluded that uptake can be manipulated, but reasons for this increase have to be further analyzed after a profiling method for the detection of 5-fluoroserotonin and other metabolites of 5-FTP has been developed.

A potential synthesis route to obtain 5-FTP is an enzymatic synthesis analogous to [^{11}C]-5-HTP. High yields in the reversed tryptophanase reaction on 5-fluoroindole indicate that the fluorine atom does not affect the enzymatic synthesis of 5-FTP from 5-fluoroindole. The pH was found to be the key factor in the enzymatic synthesis.

As a prerequisite for this approach we investigated the synthesis of 5-fluoroindole by electrophilic fluorodestannylation. Major challenge is the separation of fluoroindole from its stannylated precursor, which is used in relatively large amounts. HPLC proved to be satisfactory. We performed the enzymatic tryptophanase reaction with HPLC purified 5-fluoroindole giving 5-FTP. ^{18}F-labeling work towards [^{18}F]-5-FTP applying a similar approach is in progress.

TECHNOLOGY

4.1 Cyclotron

Statistics regarding radionuclide production of the cyclotron (Scanditronix MC-17) are presented in Fig.7 and Table 3. The figure gives an overview of cyclotron use in 2007. Average values for the whole period of use since 1992 are presented in the Table. Maintenance work was done every Monday morning before 9.30 a.m. All installation work in 2007 could be done within the scheduled maintenance time.

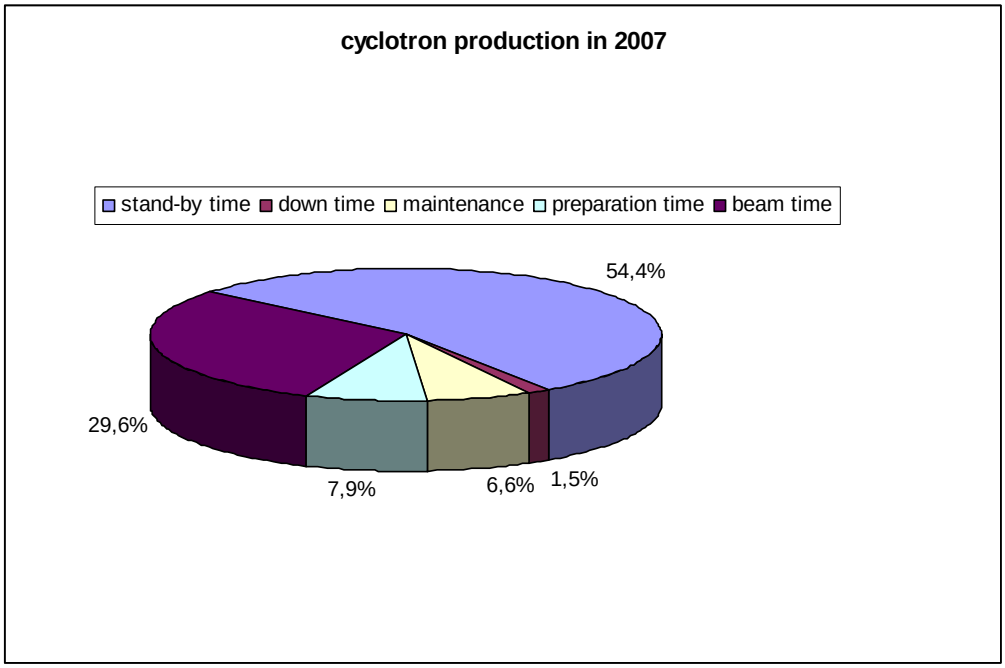

Figure 7: Cyclotron use in 2007.

Table 3. Average values for cyclotron use (2007 and previous period)

	average value (1992-2006)	**2007**
number of beams	1900	1552
beam time (hours)	557	672
Preparation time (hours)	235	180
maintenance (hours)	207	149
unscheduled down time (hours)	93	33
stand-by time (%)	50	54

Down time of the cyclotron in 2007 was 1.5 %, which is significantly lower than the average value for the period 1992-2007 (3.9 ± 2.1 %, or 88 ± 48 h). Yearly average down-time of the cyclotron is plotted in Fig.8.

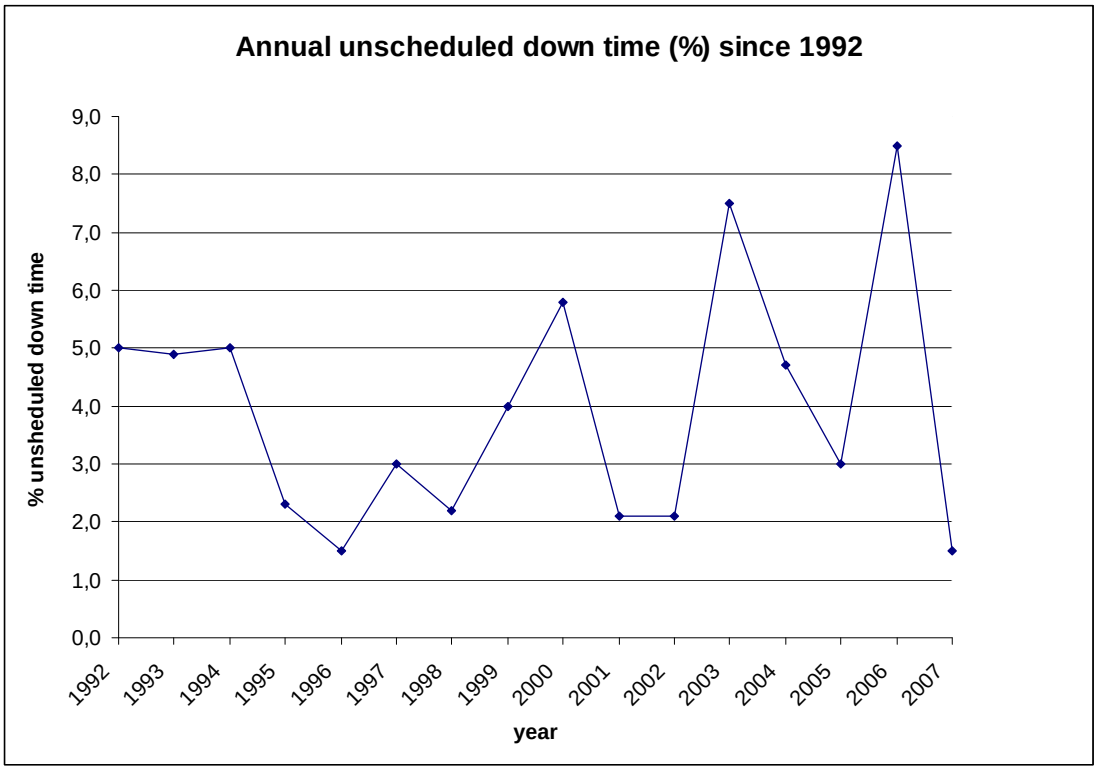

Fig.8. Yearly unscheduled down time (%) since the installation of the cyclotron

Causes underlying the 33 hours of down time in 2007 are listed in Table 4.

Table 4. Cyclotron failures in 2007

Subsystem	Hours
General (general supply hospital)	8
Magnet (gradient coils)	2
RF-system (APS)	13.5
Ion-source	-
Extraction	-
Diagnostic	-
Vacuum	-
Control	1
Target	8.5
Process system	-
Water cooling cyclotron	-

One hundred-and-forty-nine hours were required for maintenance, which included replacement or modification of the following parts:

- Upgrading of PLC software (step-5 program)
- Festo airpressure valves for the target ladder
- Replacement of the tubing for fluoride production
- Replacement of the insert of the Nuclear Interface fluoride target
- Installation of a second new fluoride target (in cooperation with Lund University, see Figs.9 and 10)
- Replacement of the foils of the $^{18}F_2$ target (1 x)
- Vacuum system: Lucifer valve and backing valve
- Replacement of tubing for the helium cooling of the targets
- Replacement of the membranes of the pump for the helium cooling (2 x)
- Replacement of the O-ring of the target-chamber (1 x)
- Bellow of the Faraday cup (2 x)

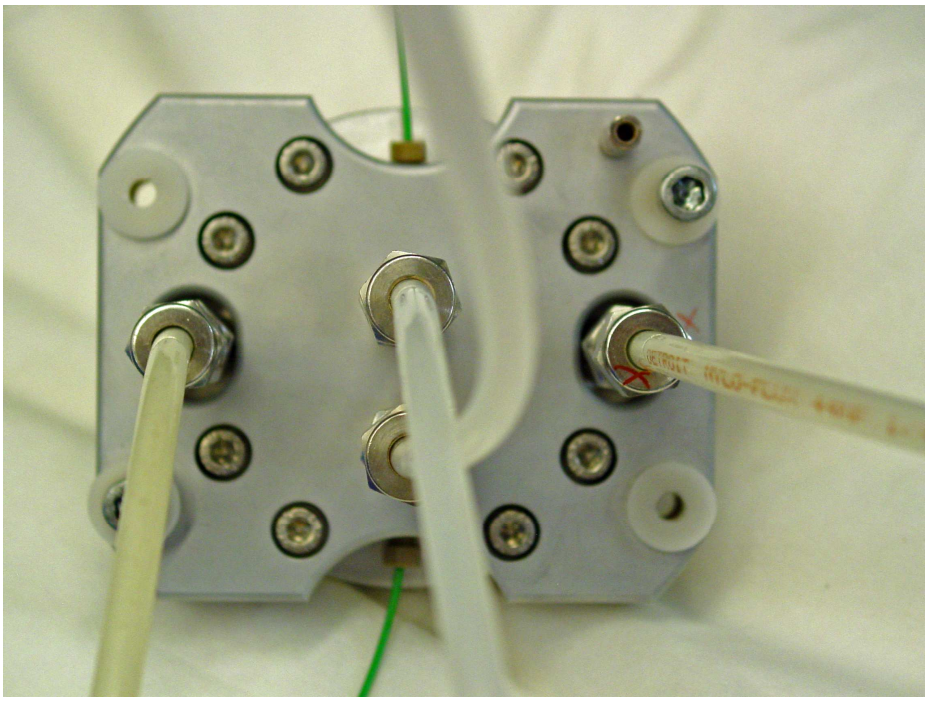

Fig.9. The second fluoride target for the MC-17, haviig a Niobium insert.

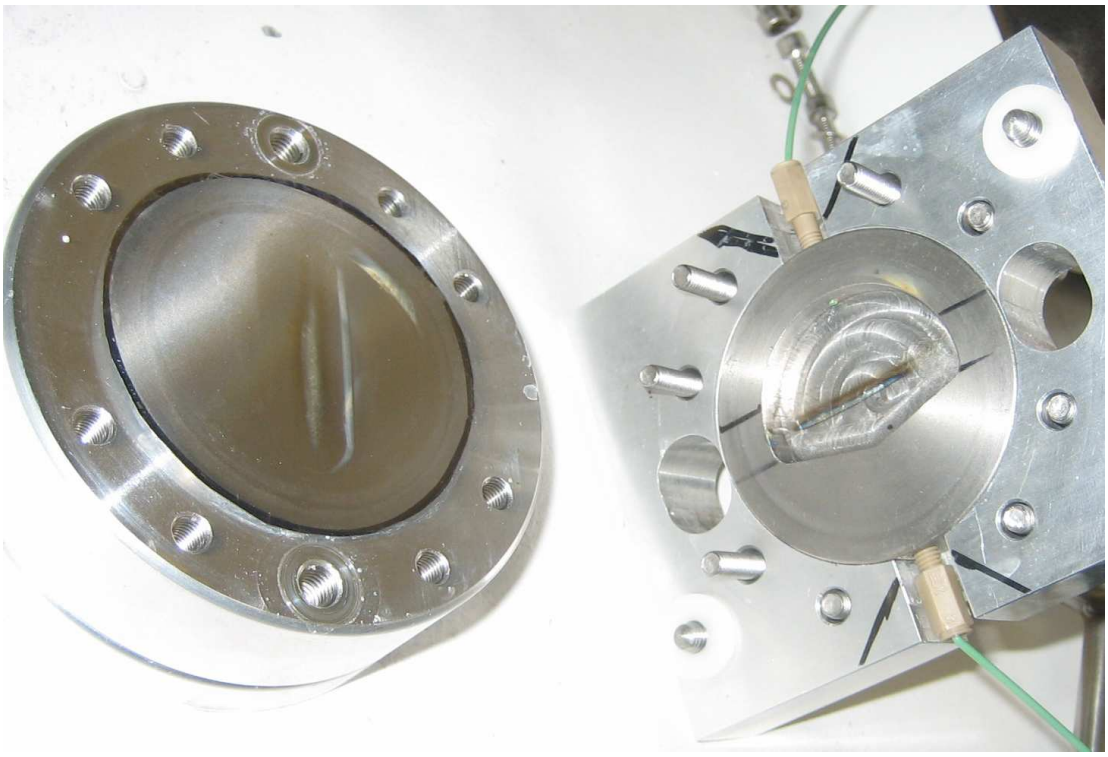

Fig.10. The original (first) Scanditronix MC-17 fluoride target. Left: Helium cooling flange with 100 µm Havar foil, right: The Niobium insert (volume 3 $cm^{3)}$, in the target body after several irradiations.

4.2 Gamma cameras and clinical PET scanners

At the present, two dual-headed gamma cameras and two single-headed gamma cameras are in use for clinical and research studies in humans. Three of the four systems show errors on a regular basis and require more than occasional maintenance. The complete single photon machine park is outdated and has to be replaced. The computer platform of the present gamma cameras is the Siemens Icon which is also out of date. Since the older PET scanner has been already acquired in 1996 it was decided that this machine should be replaced by an-up-to date PET/CT system. A combined European tender for new gamma cameras, a PET/CT system and a new computer platform for all these scanners has been published. The evaluation of the quotation has been completed and a final selection of equipment is expected in 2008. The newer PET scanner, a Siemens Ecat Exact HR+ acquired in 2004, will stay in operation for the coming years. This system is quite reliable and stable.

4.3 Facilities for small animal imaging

Our facilities for small animal imaging were expanded in 2007. All protocols for animal scanning are now examined by a special task group and a full-time biotechnician (ing.J.W.A.Sijbesma) has been appointed. The task group contains two physicists (prof.A.M.J.Paans, dr.J.R.de Jong), one radiochemist (dr.E.F.J.de Vries), one biomedical Ph.D. student (drs.W.Nagengast), the biotechnician and one biologist

(dr.A.van Waarde). The feasibility of protocols (from an imaging and radiochemistry perspective) is examined by the task group and suggestions for improvement are mailed to the investigators. Any protocol involving experimental animals and microPET or microCT scanning must pass the task group *before* it is submitted to the Animal Ethics Committee (DEC). In this way, an efficient and meaningful use of the facilities can be ensured. The task group for small animal imaging has also expanded the imaging arsenal. A BioVet system for cardiac and respiratory gating was purchased. Electronic equipment to maintain the body temperature of experimental animals within the physiological range has been acquired. Facilities for external storage of microPET data were created. A biohazard cabinet was installed in order to allow handling of genetically modified organisms. Stereotactic framers for rats have been designed and built. A website for users of the imaging facilities has been created including various checklists for potential researchers.

The appointment of a biotechnician has resulted in a central point of communication for users of the animal facilties. The biotechnician provides (bio)technical support, planning of camera time and radiopharmaceutical production, help during data acquisition and image reconstruction, and overall quality control. Because of this centralization of tasks in a single person, studies run much more smoothly than before.

4.4 MicroPET

A number of software/firmware updates has been installed in 2007. The most important change is the addition of a queuing system for reconstruction tasks. This enables users to schedule reconstructions for processing during the night. The first few iterations of the new software proved to be highly unstable. This did not result in reduced production, but it caused delays in image reconstruction and the following data analysis.

The microPET hardware has proven to be very stable. Occasional lock-ups of the system occurred very rarely, like in the previous year. No other reasons for down time can be reported. There have been no hardware malfunctions requiring parts replacement. The only maintainence required was the regular greasing of moving parts. Quality control has indicated that there is hardly any electronic drift of the system. Normalizations could therefore be performed when software updates were installed. More frequent normalizations were not required.

Stability of the acquisition software has decreased. An increasing amount of software crashes is almost certainly related to the fact that the focus of software development has changed from the microPET system to the Inveon system as well as to cluttering of the Windows registry. Yet, we have decided to postpone complete reinstallation of the operating system and software, as the stability problems are not severe and the benefits of reinstallation do not outweigh the drawbacks of protracted downtime. In 2008, a better logging of camera problems will be implemented.

4.5 MicroCAT

The number of animal studies performed on the microCAT II was smaller in 2007 than in 2006. There are several reasons for this. First, the field-of-view of the microCAT II is much smaller than that of the microPET. It is already difficult to scan a single rat and it is impossible to scan two rats simultaneously. Simultaneous scans of two rats are often performed with the microPET for logistic reasons (short half life of PET radionuclides, reduction of camera use). Second, the microCAT cannot be used for attenuation correction of the microPET data since the microPET hardware (platform for scanning 2 rats) does not fit into the CT. Finally, because of software problems it is difficult to fuse PET and CT images and to perform data analysis on the combined image.

One hardware failure of the microCAT II system occurred in 2007. This was a case of a broken shutter which has been replaced.

4.6 Overview of the small animal scans

What follows is a short summary of the scans that have been performed on both machines in 2007

The microPET system was used for studies in oncology, cardiology and basic neuroscience involving receptor binding, microglial activation, transporter activity, metabolism and blood flow The following tracers were used for this purpose: ^{18}F-FDG, ^{11}C-PK11195, ^{18}F-bombesine, ^{11}C-choline, ^{15}O-water, ^{11}C-SA5403, ^{11}C-verapamil, ^{18}F-FHBG, ^{11}C-DPA-713, ^{18}F-DPA-714, and ^{11}C-raclopride, besides the following ^{89}Zr-labeld antibodies and fragments: cetuximab, ranibizumab, Fab-IgG.. The total number of scans (each of which could involve either one or two rodents) amounted to 306: 174 rats and 132 mice. In the previous year (2006), the figures were: 358 scans in total, 188 rats and 170 mice. Since data for the number of animals per scan have not been provided, figures are not directly comparable .

The microCT has been used for scanning mice (oncology) and organs (dentistry, explanted rat jaws). Intact rats were not scanned. The total number of scans was 223 (88 on mice and 135 on tissues or other materials). In the previous year (2006), the figures were: 27 rats, 162 mice and 43 organs (232 scans in total).

4.7 Data analysis

In 2007 several developments in the analysis of brain studies culminated in a new standardized procedure which is advised for all dynamic PET brain studies. Up to now, it was common practice to first perform the various kinetic analysis methods which could then be followed by a stereotactic normalization into a standard anatomical coordinate system. Now we propose to always start with a stereotactic normalization of the dynamic PET scan and only afterwards continue with the actual data analysis e.g. by pharmacokinetic modelling.

The stereotactic normalization consists of two steps. First, if different scans are available for a single subject e.g. different PET scans or PET and MRI scans, then these are first brought into coregistration. Second, the coregistered scans of each subject are brought into a standarized space so that scans from different subjects can be compared one to one.

To coregister two PET scans which are very similar, a realignment based on for example the minimization of a chi-square error can be sufficient. However, in many cases the PET scans may be dissimilar for example because different tracers are used or because the PET scans are performed under different conditions e.g. in therapy evaluation or in receptor occupancy studies. In those cases, a coregistration is performed based on the optimization of the normalized mutual information. Since all scans are of the same subject, a rigid body transformation should be adequate. However, to allow for small errors in the pixel size and thus the apparent size of the brain, a zoom in all 3 directions is allowed. Of course the resulting zoom should be carefully checked since a zoom of more than 1-2% probably indicates an error.

The stereotactic normalization of the set of coregistered data sets requires not only a translation, rotation and zoom but also some form of non-linear warping to compensate for differences in the individual brain structures. Ideally, this should be performed based on a MRI scan since the PET scan does not show as much anatomical detail because of the specificity most tracers and the much lower spatial resolution. In either case, a template image must be available which is already in the required anatomical coordinate system.

For both the coregistration and the stereotactic normalization we used the procedures as implemented in SPM2. The practical implementation focused on two problems. <1> How to use or adapt the SPM procedures for dynamic PET scans, and <2> How to cope with the differences in file format since SPM2 uses an adapted ANALYZE format whereas the dynamic PET scans are in ECAT format and the coregistered and stereotactically normalized dynamic PET scans must also be in ECAT format for further processing.

The first problem is handled by generating a representative static image for each dynamic PET scan by summing the relevant frames. These might either be a group of end frames for maximum signal to noise ratio or a group of start frames when the PET image still represents the distribution phase of the tracer. This approach implies of course that motion during the dynamic PET scan is ignored and should thus be solved beforehand. The required transformations as determined by SPM based on this static image are then applied to the dynamic PET scan.

To handle the different file formats is not difficult per se since we have used our own translation programs for many years. However, we had to adapt them to handle dynamic PET scans and conserve the origin of the data after stereotactic normalization. Also, since we are changing between different file formats and programming environments we had to be careful about the left-right orientation. This was checked using scans with markers or a left-right asymmetry.

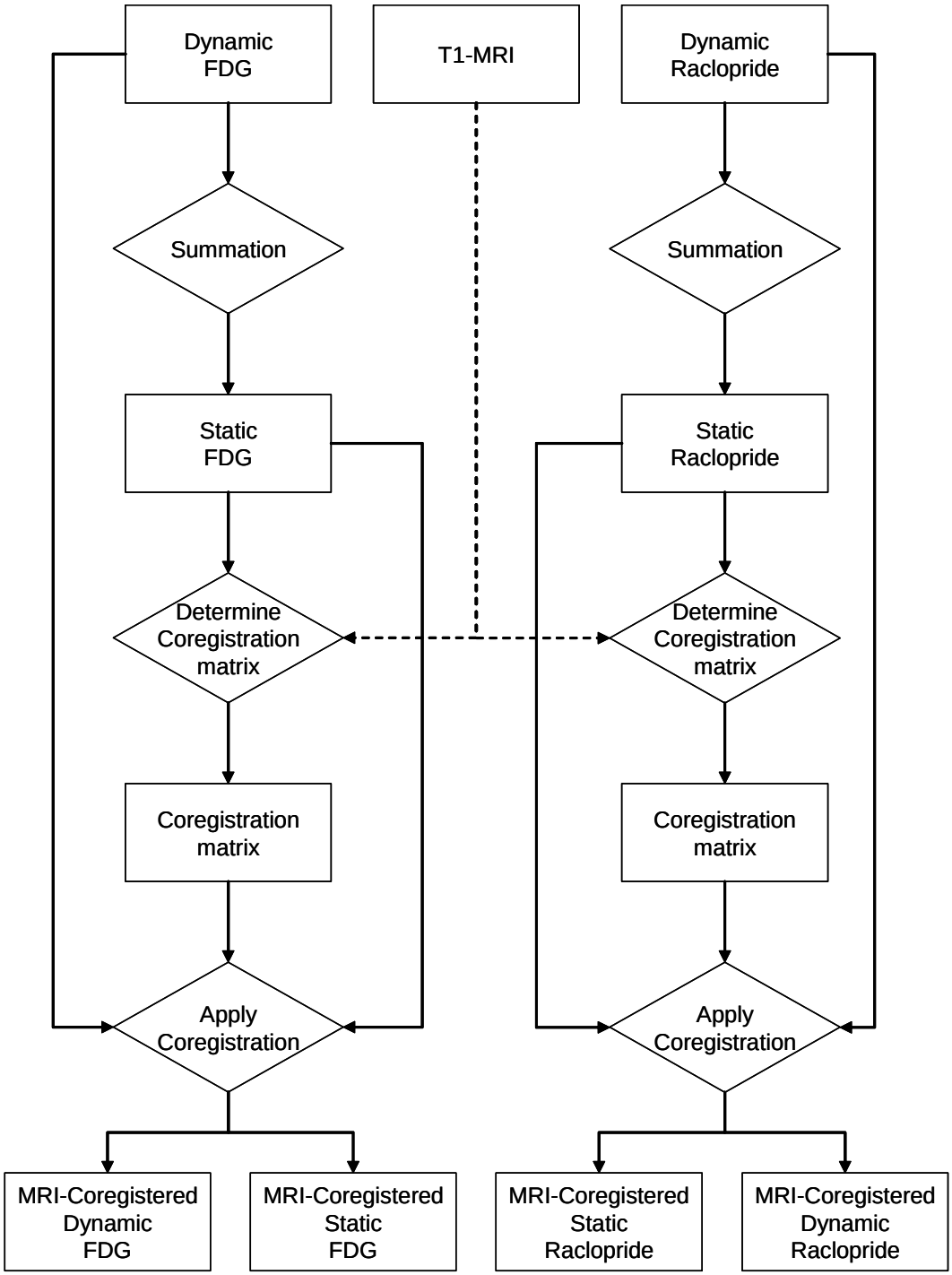

Figure 11. Independent coregistration of an FDG and a Raclopride PET scan of a single subject with the subjects' own T1-MRI. The coregistration parameters are determined using static, summed, images of FDG and Raclopride.

As an example, we consider the coregistration and normalization of a study in which a dynamic FDG and Raclopride PET scan were acquired as well as a T1-MRI. Figure 11 shows the flow diagram for the coregistration of the PET scans with the MRI scan. In this example, the coregistrations of the FDG and the Raclopride scans are independent of each other thus two separate coregistration matrices are determined. Each coregistration matrix is then applied to the dynamic as well as the static,

summed, PET scans. The MRI-coregistered PET scans can than be normalized into a stereotactic reference coordinate system as shown in Figure 12.

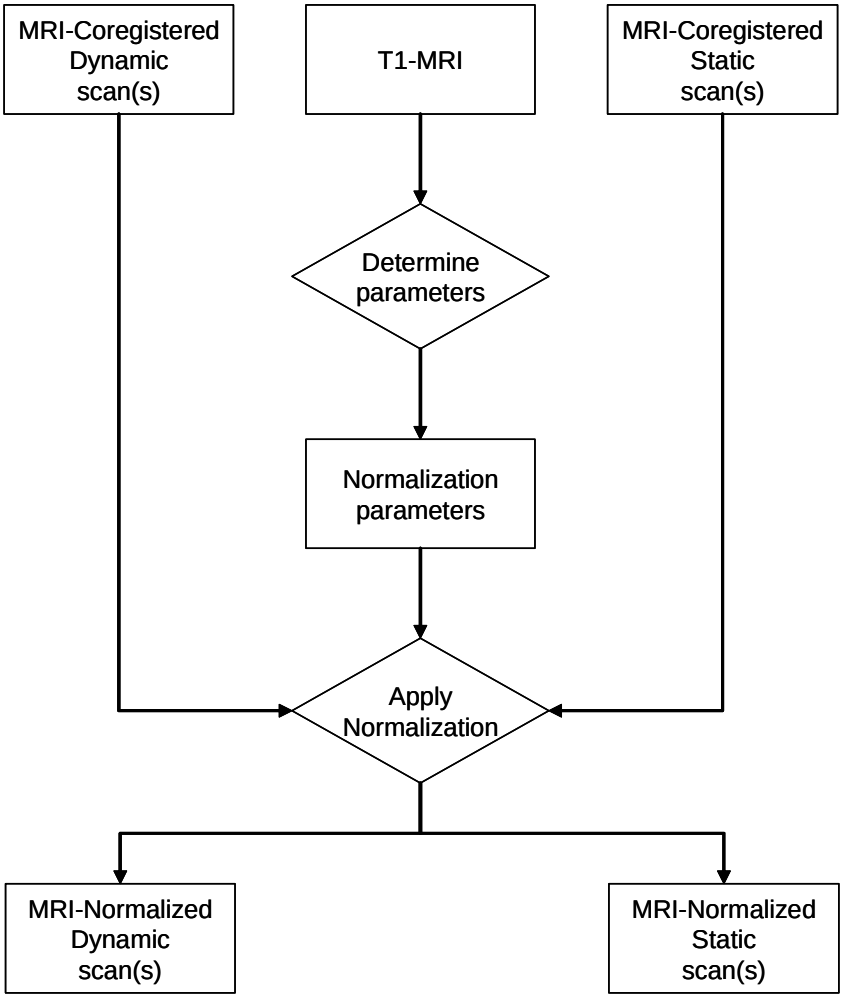

Figure 12. Stereotactic normalization of MRI-coregistered PET scans using the subject specific T1-MRI scan.

After stereotactic normalization, all scans of all subjects should be in exactly the same space i.e. each voxel of each scan should represent exactly the same anatomical area. In practice, this will never be fully realized. However, since the normalization is based on the high resolution MRI scan and the PET scan has a much lower resolution this will probably be true in practice. In this respect, the use of a single set of normalization parameters is advantageous since this ensures that the stereotactic normalization does not introduce additional variability. Thus the variability is determined only by the MRI-coregistration as shown in Figure 11.

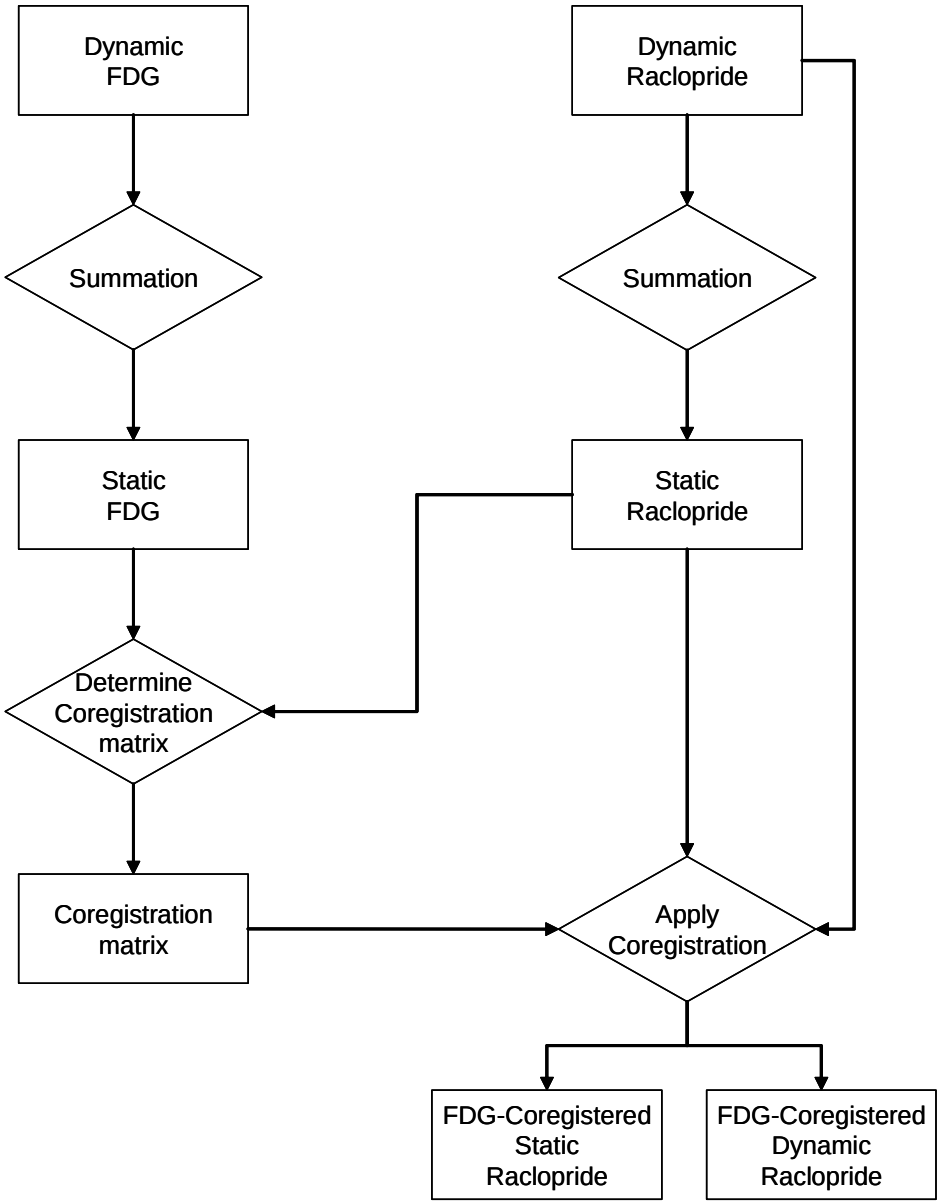

Figure 13. Coregistration of dynamic Raclopride scans with a dynamic FDG scan.

The application of two independent coregistrations may thus not be optimal. Depending on the tracers used it may actually be better to first coregister the two or more PET scans and then use one of them for the coregistration with the MRI. The first step of this alternative approach is shown in Figure 13. Since the FDG scan shows more anatomical structure, it is better suited for the ensuing coregistration with the T1-MRI scan. Therefore, in this example, the raclopride scans are coregistered to the FDG scans. The coregistration of the FDG scans together with the FDG-coregistered raclopride scans can then proceed as shown in Figure 14.

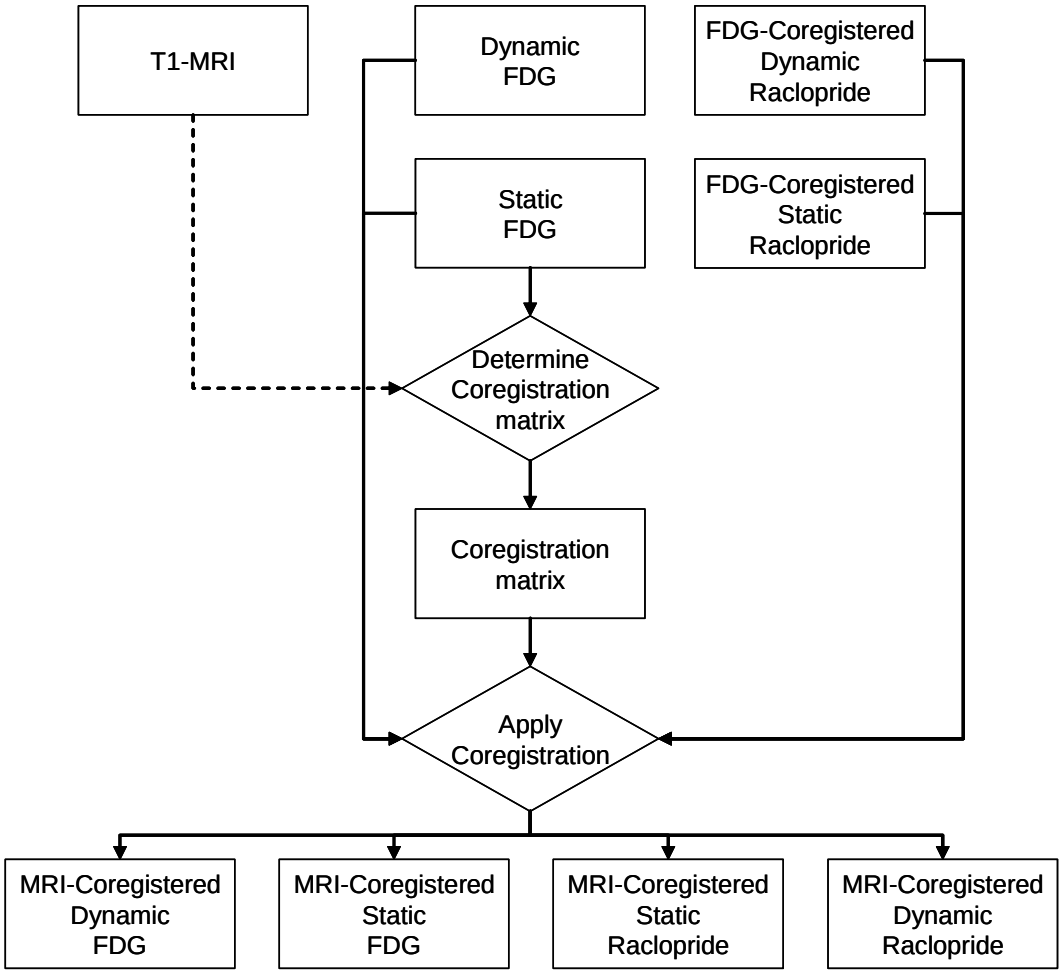

Figure 14. Coregistration of an FDG PET scan with a T1-MRI. The raclopride scans were previously coregistered to this FDG scan (cf Fig 13). Thus only a single MRI-FDG based coregistration matrix is used for the coregistration of all PET scan.

The resulting coregistered PET scans can then be normalized into a standard reference coordinate system as already discussed above and shown in Figure 12. Note that in this approach, as mentioned above, intra-individual differences can only occur in the coregistration of the raclopride scans with the FDG scan since the coregistration with the MRI scan and the stereotactic normalization use identical parameter sets for all PET scan.

Note that this approach can also be applied if the PET scans are acquired at different time-points. In those cases where a specific tracer is used several times, where the time between scans may be just hours or even several years, one could also first coregister the PET scans, determine the mean images and use these for the coregistration to the MRI and the normalization based on the MRI. When an MRI scan is not available, one can still use the coregistration techniques, however in these cases the normalization must be based on the PET scans themselves and a normalized PET template must be available.

Since in this approach, i.e. first normalizing the data as discussed in some detail above, the data of all subjects should have the same spatial coordinate system one can

now also easily perform a group analysis either on a pixel by pixel basis or at a ROI level. For the pixel by pixel analysis, one would normally first perform some pixel by pixel calculation of for example the distribution volume or the binding potential followed by for example a SPM like analysis. For the ROI analysis, two approaches can be followed. First, for those models which can be employed on a pixel by pixel basis one can apply the model and then determine the average values per ROI. Secondly, one can first determine the average time-activity curve per ROI and then apply the kinetic model. The advantage of the latter approach is of course that more models are available. The disadvantage is then of course that this approach does not allow a SPM like analysis. To facilitate either approach two additional programs were written. The first enables the projection of individual or groups of ROIs on the normalized images and can be used to visually assess the quality of the normalization. The second program accepts either static or dynamic PET scans and calculates the average values for each ROI for each frame. So for a distribution volume image this will give the distribution volume per volume. For a dynamic PET scan this will give the time-activity curve per ROI. The output is a text file which can easily be imported into a spreadsheet program. The programs available at the UMCG for pharmacokinetic modeling were adapted also to read the resulting time-activity curves.

Although the use of different programs and different file formats limit the work-flow, the methods made available are straight-forward to use provided that procedures are strictly followed. For those who understand the methodology and the rationale behind the choices made, the methods actually provide a very flexible and powerful set of tools which can be used in many different studies.

4.8 Radionuclide and radiopharmaceutical production

The production values for the various radionuclides are presented in Table 5.

Table 5: Production of radionuclides in 2007.

Nuclide	Irradiations	Irradiation time (h)	Mean irradiation time (min)	Total activity (GBq)
^{15}O	102	2.3	1.3	336
^{13}N	179	34.6	11.6	1234
^{11}C	553	240.1	26.0	31317
$^{18}F^-$	336	130.9	23.4	9008
$^{18}F_2$	382	264.3	41.5	2724

Fourteen PET radiopharmaceuticals were used for clinical studies in 2007. An overview of the entire tracer production since 1992 is given in Table 6

	2007	*2006*	*2005*	*2004*	*2003*	*2002*	*2001*	*2000*	*1999*	*1998*	*1997*	*1996*	*1995*	*1994*	*1993*	*1992*
1. ^{18}F-FDG	**262**	225	272	251	239	219	222	200	210	191	147	101	95	105	110	82
2. $^{13}NH_3$	**144**	73	50	210	160	200	222	461	381	432	566	536	313	273	204	225
3. ^{18}F-Dopa	**128**	134	99	104	66	50	59	42	50	41	-	-	-	-	-	-
4. ^{11}C-Methionine	**48**	38	29	22	16	6	-	-	-	-	-	-	-	-	-	-
5. ^{11}C-Raclopride	**43**	3	32	18	30	61	49	25	11	9	-	-	-	-	-	-
6. ^{11}C-PK11195	**38**	-	-	-	-	-	-	-	-	-	-	-	-	-	-	-
7. ^{11}C-HTP	**37**	60	7	-	-	-	-	-	-	-	-	-	-	-	-	-
8. $H_2{}^{15}O$	**30**	126	538	393	507	245	491	557	448	216	234	724	581	629	290	154
9. ^{11}C-Choline	**21**	28	30	26	22	13	22	57	35	31	-	-	-	-	-	-
10. ^{18}F-FLT	**19**	8	12	31	46	56	11	-	-	-	-	-	-	-	-	
11. ^{11}C-mHED	**10**	-	-	-	-	-	-	-	-	-	-	-	-	-	-	-
12. ^{11}C-Verapamil	**4**	30	40	-	2	24	14	15	10	-	2	-	-	-	-	-
13. ^{18}F-NaF	**2**	3	16	19	-	-	-	-	-	-	-	-	-	-	-	-
14. ^{11}C-SA4503	**1**	21	3	-	-	-	-	-	-	-	-	-	-	-	-	-
15. ^{15}O-CO	-	-	4	-	-	-	-	1	5	4	4	11	17	-	-	-
16. ^{18}F-FMISO	-	-	2	2	2	2	2	-	-	-	-	-	-	-	-	-
17. ^{18}F-FHBG	-	4	1	-	-	-	-	-	-	-	-	-	-	-	-	-
18. ^{11}C-CGP-12388	-	-	-	4	3	13	9	12	6	2	-	-	-	-	-	-
19. ^{11}C-Carvedilol	-	-	-	1	2	-	-	-	-	-	-	-	-	-	-	
20. ^{11}C-Tyrosine	-	-	-	-	-	11	42	35	32	57	83	148	158	147	39	9
21. ^{18}F-MPPF	-	-	-	-	-	9	9	8	10	2	-	-	-	-	-	-
22. ^{11}C-Acetate	-	-	-	-	-	-	2	8	2	8	27	19	29	-	-	-
23. ^{11}C-VC002	-	-	-	-	-	-	-	-	-	2	4	2	-	-	-	-
24. ^{18}F-Fluorcarazolol	-	-	-	-	-	-	-	-	-	-	-	5	14	3	-	-
25. ^{11}C-Thymidine	-	-	-	-	-	-	-	-	-	-	-	-	7	13	13	-
26. ^{18}F-FESP	-	-	-	-	-	-	-	-	-	-	-	-	-	9	-	-
27. ^{11}C-CGP-12177	-	-	-	-	-	-	-	-	-	-	-	-	-	16	6	-
28. ^{11}C-Bicarbonate	-	-	-	-	-	11	34	12	-	-	-	-	-	-	-	-

Table 6: Overview of the entire tracer production (for clinical use) in the period 1992-2007
Radiopharmaceuticals printed in bold are currently in routine production.

PUBLICATIONS 2007

5.1 Ph.D.Theses and Books

1. De Boer, JR. Clinical Applications of L-[1-^{11}C]-tyrosine PET in laryngeal cancer. [Promotores: F.W.J.Albers, **W.Vaalburg;** copromotores: B.F.A.M.van der Laan, **J.Pruim]** Ph.D.Thesis, University of Groningen, March 7, 2007. 112 pages.

2. Doting MHE. Sentinel lymph node biopsy in breast cancer and melanoma. [Promotores: H.J.Hoekstra, copromotores: J.de Vries, **P.L.Jager]** Ph.D.Thesis, University of Groningen, March 7, 2007. 134 pages.

3. Georgiadis JR. The Orgasmic Brain Exposed. [Promotores: **R.A.J.O.Dierckx, A.M.J.Paans;** copromotor: R.Kortekaas] Ph.D.Thesis, University of Groningen, May 30, 2007. 160 pages.

4. Hazenberg BPC. Diagnostic studies in amyloidosis. [Promotores: M.H.van Rijswijk, P.C.Limburg; copromotor: **P.L.Jager]** Ph.D.Thesis, University of Groningen, November 28, 2007. 198 pages. *[nuclear medicine techniques were used in this thesis]*

5. Mansour K. Clinical investigation in the diagnosis and treatment of the dry and wet eye. [Promotor: J.M.M.Hooymans, co-promotores L.J.Blanksma, **P.L.Jager**] Ph.D.Thesis, University of Groningen, September 12, 2007. 184 pages. *[dacryoscintigraphy, a nuclear medicine technique, was used in this thesis]*

6. **Phan TTH.** Imaging Strategy in Differentiated Thyroid Cancer. [Promotores: **R.A.J.O.Dierckx,** B.H.R.Wolffenbuttel, **P.L.Jager]** Ph.D.Thesis, University of Groningen, November 26, 2007. 148 pages.

7. Schot BW. Positron emission tomography in malignant haematological disease. [Promotores: E.Vellenga, **W.Vaalburg**] Ph.D.Thesis, University of Groningen, October 10, 2007. 133 pages.

8. **Signore A.** Radiolabelled interleukin 2 for in vivo imaging of activated T-lymphocytes. [Promotores: **R.A.J.O.Dierckx, C.van de Wiele]** Ph.D.Thesis, University of Groningen, March 7, 2007. 144 pages.

5.2 M.Sc.Theses etc

1. **Fiebrich HB.** Diagnostic value of ^{18}F-DOPA in patients with pheochromocytoma. Wetenschappelijk stageverslag co-assistentschap, supervisors: De Vries EGE, **Brouwers AH,** Links TP] Groningen 2007.

2. Keimpema E. PET imaging of activated microglia in neurodegenerative disorders with the radioligand [^{11}C]PK11195. M.Sc.thesis, in cooperation with Dept.Biology, University of Groningen, Haren, The Netherlands. 2007. 27 pages [supervisor: **van Waarde A]**

3. Muskiet E. De waarde van CT/SPECT fusie in de preoperatieve lokalisatie van bijschildkliertumoren bij patiënten met hyperthyreoïdie. Wetenschappelijk stageverslag co-assistentschap, supervisors: Plukker JTM, **Brouwers AH]** Groningen 2007.

4. **Kruizinga S.** PET as a tool for monitoring radiation-induced inflammation and radiosensitization. M.Sc.thesis, in cooperation with VU Medisch Centrum, Free University of Amsterdam. 2007. 31 pages. [supervisors: **De Vries EFJ, Van Waarde A,** Bijl H].

5. N.N. Samenvoeging zorgadministraties NGMB. Aan welke aspecten van de structuur en cultuur bij de zorgadministraties moet het management aandacht besteden, gezien de strategie van het kwaliteitsbeleid van de afdeling NGMB? [Afstudeer stageverslag opleiding personeelsmanagement, supervisors: **Brouwers AH, Medema J,** Van Kempen J]. Groningen 2007.

6. **Vellinga NAR.** Imaging P-glycoprotein function and neuroinflammation in the rat brain with positron emission tomography (PET). M.Sc.thesis, 2007. [supervisors: **De Vries EFJ, Klein HC, Doorduin J].**

5.3 Papers in international journals

1. **Annovazzi A,** Amendolia SR, Bigongiari A, Bisogni MG, Catarsi F, Cesqui F, Cetronio A, Colombo F, Delogu P, Fantucci ME, Gilberti A, Lanzieri C, Lavagna S, Novelli M, Passuello G, Paternoster G, Pieracci M, Poletti M, Quattrocchi M, Rosso V, Stefanini A, Testa A, Venturelli L. A GaAs pixel detectors-based digital mammographic system: Performances and imaging tests results. Nucl Inst Meth Phys Res Sect A 2007; 576:154-9.

2. **Bart J, Nagengast WB,** Coppes RP, **Wegman TD,** van der Graaf WT, Groen HJ, **Vaalburg W,** de Vries EG, **Hendrikse NH.** Irradiation of rat brain reduces P-glycoprotein expression and function.Br J Cancer. 2007;97:322-6.

3. **Been LB,** Suurmeijer AJ, **Elsinga PH, Jager PL,** van Ginkel RJ, Hoekstra HJ. ^{18}F-fluorodeoxythymidine PET for evaluating the response to hyperthermic isolated limb perfusion for locally advanced soft-tissue sarcomas. J Nucl Med. 2007;48:367-72.

4. Beerens AM, Rots MG, **de Vries EF**, Haisma HJ. Fusion of herpes simplex virus thymidine kinase to VP22 does not result in intercellular trafficking of the protein. Int J Mol Med. 2007;19:841-9

5. Burroni L, D'Alessandria C, **Signore A.** Diagnosis of vascular prosthesis infection: PET or SPECT? J Nucl Med. 2007;48:1227-9.

6. Buscombe JR, **Signore A**. Has radio-targeting come of age? Report of the 18th IRIST meeting. Q J Nucl Med Mol Imaging. 2007;51:290-1.

7. Czepczyński R, Parisella MG, Kosowicz J, Mikołajczak R, Ziemnicka K, Gryczyńska M, Sowiński J, **Signore A.** Somatostatin receptor scintigraphy using ^{99m}Tc-EDDA/HYNIC-TOC in patients with medullary thyroid carcinoma. Eur J Nucl Med Mol Imaging. 2007;34:1635-45.

8. D'Alessandria C, Malviya G, Viscido A, Aratari A, Maccioni F, Amato A, Scopinaro F, Caprilli R, **Signore A.** Use of a ^{99m}Tc labeled anti-TNFalpha monoclonal antibody in Crohn's disease: in vitro and in vivo studies. Q J Nucl Med Mol Imaging. 2007;51:334-42.

9. Dasselaar JJ, **Lub-de Hooge MN, Pruim J, Nijnuis H,** Wiersum A, de Jong PE, Huisman RM, Franssen CF. Relative blood volume changes underestimate total blood volume changes during hemodialysis. Clin J Am Soc Nephrol. 2007;2:669-74.

10. De Geus-Oei LF, Van der Heijden HF, Visser EP, Hermsen R, Van Hoorn BA, Timmer-Bonte JN, **Willemsen AT, Pruim J,** Corstens FH, Krabbe PF, Oyen WJ. Chemotherapy response evaluation with ^{18}F-FDG PET in patients with non-small cell lung cancer. J Nucl Med. 2007;48:1592-8.

11. De Jong BM, **Paans AM.** Medial versus lateral prefrontal dissociation in movement selection and inhibitory control. Brain Res. 2007;1132:139-47.

12. De Jong WK, van der Heijden HF, **Pruim J,** Dalesio O, Oyen WJ, Groen HJ. Prognostic value of different metabolic measurements with fluorine-18 fluorodeoxyglucose positron emission tomography in resectable non-small cell lung cancer: a two-center study. J Thorac Oncol. 2007;2:1007-12.

13. De Korte MA, de Vries EG, **Lub-de Hooge MN, Jager PL**, Gietema JA, van der Graaf WT, Sluiter WJ, van Veldhuisen DJ, Suter TM, Sleijfer DT, Perik PJ. ^{111}Indium-trastuzumab visualises myocardial human epidermal growth factor receptor 2 expression shortly after anthracycline treatment but not during heart failure: a clue to uncover the mechanisms of trastuzumab-related cardiotoxicity. Eur J Cancer. 2007;43:2046-51.

14. **De Vries EF**, Rots MG, Hospers GA. Nuclear imaging of hormonal receptor status in breast cancer: a tool for guiding endocrine treatment and drug development. Curr Cancer Drug Targets. 2007;7:510-9.

15. Doting MHE, **Stiekema HMA,** De Vries J, **Lemstra C,** Hoekstra HJ, Vrieling M, Rietman L, **Jager PL.** Immediate dynamic lymphoscintigraphy delivers no additional value to lymphoscintigraphy 3 hr after tracer injection in sentinel lymph node biopsy in breast cancer patients. J Surg Oncol 2007;45:469-75.

16. Doting MHE, de Vries M, Plukker JT, **Jager PL,** Post WJ, Suurmeijer AJ, Hoekstra HJ. The value of sentinel lymph node biopsy in the management of head and neck melanoma [Letter]. J Surg Oncol 2007;95:523.

17. Geluk CA, Dikkers R, Kors JA, Tio RA, **Slart RH,** Vliegenthart R, Hillege HL, Willems TP, de Jong PE, van Gilst WH, Oudkerk M, Zijlstra F. Measurement of coronary calcium scores or exercise testing as initial screening tool in asymptomatic subjects with ST-T changes on the resting ECG: an evaluation study. BMC Cardiovasc Disord. 2007;7:19.

18. Georgiadis JR, **Reinders AA,** Van der Graaf FH, **Paans AM,** Kortekaas R. Brain activation during human male ejaculation revisited. Neuroreport. 2007;18:553-7.

19. Goethals I, Verraet M, Audenaert K, Jacobs F, Ham H, **Van de Wiele C,** Vandecapelle M, Slegers G, **Dierckx R,** Van Heeringen C. Differences of cortical 5-HT2A receptor binding index with SPECT in subtypes of anorexia nervosa: Relationship with personality traits? J Psychiat Res 2007; 41:455-8.

20. Greupink R, Reker-Smit C, Proost JH, van Loenen Weemaes AM, **de Hooge M**, Poelstra K, Beljaars L. Pharmacokinetics of a hepatic stellate cell-targeted doxorubicin construct in bile duct-ligated rats. Biochem Pharmacol. 2007;73:1455-62.

21. Hazenberg BP, van Rijswijk MH, **Lub-de Hooge MN**, Vellenga E, Haagsma EB, Posthumus MD, **Jager PL.** Diagnostic performance and prognostic value of extravascular retention of ^{123}I-labeled serum amyloid P component in systemic amyloidosis. J Nucl Med. 2007;48:865-72.

22. Ishiwata K, Kimura Y, **De Vries EFJ, Elsinga PH**. PET tracers for mapping adenosine receptors as probes for diagnosis of CNS disorders and development of therapeutics. CNS Agents Med. Chem. 2007;7:57-77.

23. Jorna FH, **Jager PL**, Que TH, **Lemstra C**, Plukker JT. Value of ^{123}I-subtraction and single-photon emission computed tomography in addition to planar ^{99m}Tc-MIBI scintigraphy before parathyroid surgery. Surgery Today 2007;37:1033-1041.

24. Kosterink JG, McLaughlin PM, **Lub-de Hooge MN,** Hendrikse HH, van Zanten J, van Garderen E, Harmsen MC, de Leij LF. Biodistribution studies of epithelial cell adhesion molecule (EpCAM)-directed monoclonal antibodies in the EpCAM-transgenic mouse tumor model. J Immunol. 2007;179:1362-8.

25. Malviya G, **De Vries EFJ, Dierckx RA, Signore A**. Radiopharmaceuticals for imaging chronic lymphocyte inflammation. Braz Arch Biol Technol 2007;50:1-13.

26. **Nagengast WB,** de Vries EG, Hospers GA, Mulder NH, **de Jong JR,** Hollema H, **Brouwers AH,** van Dongen GA, Perk LR, **Lub-de Hooge MN.** In vivo VEGF imaging with radiolabeled bevacizumab in a human ovarian tumor xenograft. J Nucl Med. 2007;48:1313-9.

27. Persoon AC, **Jager PL**, Sluiter WJ, Plukker JT, Wolffenbüttel BH, Links TP. A sensitive Tg assay on rhTSH stimualted Tg: what's the best in the long-term follow-up of patients with differentiated thyroid carcinoma? PLOS One 2007;2:e816.

28. Pétillot P, Lahorte C, Bonanno E, **Signore A,** Lancel S, Marchetti P, Vallet B, Slegers G, Neviere R. Annexin V detection of lipopolysaccharide-induced cardiac apoptosis. Shock. 2007;27:69-74.

29. **Phan HT, Jager PL,** Plukker JT, Wolffenbuttel BH, **Dierckx RA**, Links TP. Detection of bone metastases in thyroid cancer patients: bone scintigraphy or ^{18}F-FDG PET? Nucl Med Commun. 2007;28:597-602.

30. Pietersen CY, Bosker FJ, **Doorduin J,** Jongsma ME, Postema F, Haas JV, Johnson MP, Koch T, Vladusich T, Den Boer JA. An animal model of emotional blunting in schizophrenia. PLOS One 2007;2:e1360.

31. Rachmawati H, Reker-Smit C, **Lub-de Hooge MN**, van Loenen-Weemaes A, Poelstra K, Beljaars L. Chemical modification of interleukin-10 with mannose 6-phosphate groups yields a liver-selective cytokine. Drug Metab Dispos. 2007;35:814-21.

32. Renard V, Staelens L, **Signore A**, Van Belle S, **Dierckx RA, Van De Wiele C**. Iodine-123-interleukin-2 scintigraphy in metastatic hypernephroma: a pilot study. Q J Nucl Med Mol Imaging. 2007;51:352-6.

33. Ronga G, Ventroni G, Montesano T, Filesi M, Ciancamerla M, Di Nicola AD, Travascio L, Vestri AR, **Signore A.** Sensitivity of [^{99m}Tc]methoxyisobutylisonitrile scan in patients with metastatic differentiated thyroid cancer. Q J Nucl Med Mol Imaging. 2007;51:364-71.

34. Rottey S, Loose D, Vakaet L, Lahorte C, Vermeersch H, Van Belle S, **Van De Wiele C.** ^{99m}Tc-HYNIC Annexin-V imaging of tumors and its relationship to response to radiotherapy and/or chemotherapy. Q J Nucl Med Mol Imaging. 2007; 51:182-8.

35. Rottey S, **Signore A, Van De Wiele C.** Radiolabelled chemotherapeutics. Q J Nucl Med Mol Imaging. 2007;51:139-51.

36. **Ruytjens L,** Albers F, van Dijk P, Wit H, **Willemsen AT.** Activation in primary auditory cortex during silent lipreading is determined by sex. Audiol Neurootol. 2007;12:371-7.

37. **Ruytjens L,** Georgiadis JR, Holstege G, Wit HP, Albers FW, **Willemsen AT.** Functional sex differences in human primary auditory cortex. Eur J Nucl Med Mol Imaging. 2007;34:2073-2081.

38. Schot BW, Zijlstra JM, Sluiter WJ, van Imhoff GW, **Pruim J, Vaalburg W,** Vellenga E. Early FDG-PET assessment in combination with clinical risk scores determines prognosis in recurring lymphoma. Blood. 2007;109:486-91.

39. **Udo de Haes JI**, Maguire RP, **Jager PL, Paans AM**, den Boer JA. Methylphenidate-induced activation of the anterior cingulate but not the striatum: a [^{15}O]H2O PET study in healthy volunteers. Hum Brain Mapp. 2007;28:625-35.

40. Van Dongen GAMS, Visser GWM, **Lub-De Hooge MN,** De Vries EGE, Perk LR. Immuno-PET: A Navigator in Monoclonal Antibody Development and Applications. The Oncologist 2007;12:1379-1389.

41. **Van Waarde A,** Shiba K, **De Jong JR,** Ishiwata K, **Dierckx RA, Elsinga PH.** Rapid reduction of sigma1-receptor binding and ^{18}F-FDG uptake in rat gliomas after in vivo treatment with doxorubicin. J Nucl Med. 2007;48:1320-6.

42. Van Westreenen HL, Westerterp M, Sloof GW, Groen H, Bossuyt PMM, **Jager PL,** Comans EF, Van Dullemen HM, Fockens P, Stoker J, Van der Jagt EJ, Van Lanschot JJB, Plukker JTM. Limited additional value of positron emission tomography in staging oesophageal cancer. Br J Surg 2007; 94:1515-20.

43. Westerterp M, **Pruim J,** Oyen W, Hoekstra O, **Paans A,** Visser E, van Lanschot J, Sloof G, Boellaard R. Quantification of FDG PET studies using standardised uptake values in multi-centre trials: effects of image reconstruction, resolution and ROI definition parameters. Eur J Nucl Med Mol Imaging. 2007;34:392-404.

5.4 Papers in international journals (by users of the NGMB facilities)

1. Gielkens PF, Bos RR, Raghoebar GM, Stegenga B. Is there evidence that barrier membranes prevent bone resorption in autologous bone grafts during the healing period? A systematic review. Int J Oral Maxillofac Implants 2007;22:390-8. *[1st author Pepijn Gielkens performed microCT studies in our institution]*

5.5 Papers in Dutch journals / News Reports

1. Balink H, Krabbe CA, de Visscher JGAM. De waarde van PET/ CT-onderzoek bij maligne tumoren in het hoofd-halsgebied. Ned Tijdschr Geneeskd. 2007;151:1167-72

2. Bongers V, **Brouwers AH.** CBO-richtlijn niercelcarcinoom. Tijdschr Nucl Geneeskd 2007; 29:104-106.

3. Cramer MJM**, Slart RHJA**. De werkgroep nucleaire cardiologie, MRI en MSCT van de Nederlandse Vereniging voor Cardiologie. Tijdschr Nucl Geneeskd, 2007; 29(4):173.

4. Goodman A. In pilot study, PET antibody identifies clear-cell renal cancer, potentially avoiding need for kidney biopsy. News Center Hematology, Oncology, Nursing and Pharmacy 2007; August 10:38-39. [contains interview with **Brouwers AH]**

5. Noordzij MJ, De Heide LJ, Links TP, **Jager PL,** Wolfenbuttel BH. Four patients with incidentalomas of the thyroid discovered on ^{18}F-fluoro-deoxyglucose positron-emission tomography (FDG-PET). Ned Tijdschr Geneeskd 2007; 151:2337-2341.

6. Verbeek DE, Hazenberg BP, **Jager PL,** Kremer Hovinga TK. AL-amyloidosis and its treatment by eliminating the precursor protein. Ned Tijdschr Geneeskd 2007; 151:2021-2026

7. Zeebregts CJ, Boersma HH, Rudd JHF, Hofstra L, **Slart RHJA**. Het afbeelden van de vulnerabele plaque bij vaataandoeningen. Tijdschr Nucl Geneeskd, 2007; 29(4):166-168.

5.6 Abstracts in international journals

1. Conti V, Petramala L, Cotesta D, Borianno E, Annovazzi G, **Signore A,** De Toma G, Letizia C. Endothelin (ET-1) and adrenomedullin (AM) concentration with atherosclerosis. J Hypertension 25 (Suppl 2):S57, 2007.

2. De Decker M, Bacher K, Slegers G, **Dierckx RA,** De Vos F. Formulation optimization of water-in-oil emulsion containing $^{99m}TcO_4^-$/$^{188}ReO_4^-$ for hepatoma targeting. Eur J Nucl Med Mol Imaging 34(Suppl 2):S333,2007

3. De Geus-Oei L, Van der Heijden HFM, Visser EP, Hermsen R, Van Hoorn BA, Timmer-Bonte JN, **Willemsen AT, Pruim J,** Corstens FHM, Krabbe PFM, Oyen WG. Chemotherapy response evaluation with FDG-PET in patients with non-small-cell lung cancer. Eur J Nucl Med Mol Imaging 34(Suppl 2):S143,2007

4. **De Vries EFJ, Doorduin J, Van Waarde A, Dierckx RA.** [^{11}C]Rofecoxib as PET tracer for COX-2: Evaluation in a HSV encephalitis model. J Label Comp Radiopharm 50(Suppl 1):S383,2007

5. **Dijkers ECF, Lub-de Hooge MN,** Kosterink JG, **Jager PL, Brouwers AH,** Perk LR, Van Dongen GA, De Vries EGE. Characterization of ^{89}Zr-trastuzumab for clinical HER2 immunoPET imaging. J Clin Oncol 25(18S):3508,2007

6. **Doorduin J, De Vries EFJ, Dierckx RA, Klein HC.** PET imaging of herpes simplex encephalitis in rats. J Label Comp Radiopharm 50(Suppl 1):S60,2007

7. **Doorduin J, Klein HC,** James M, Kassiou M, **Dierckx RA, De Vries EFJ.** [^{18}F]DPA-714 as a novel PET tracer for PBR: A comparison with [^{11}C]PK11195 in a rat model of HSV encephalitis. J Label Comp Radiopharm 50(Suppl 1):S333,2007

8. Elsinga PH. Design and synthesis of PET-radiopharmaceuticals. [invited lecture, CME8: Radiopharmacy, Pharmacokinetic modeling]. Eur J Nucl Med Mol Imaging 34(Suppl 2):S191,2007.

9. Jager PL, Stiekema AM, Jonkman S, Koolhaas W, Wolffenbuttel BH, **Slart RH,** Webber CE, Gulenchyn KY. Instant vertebral assessment (IVA) in combination with bone densitometry (BDM): A new standard in the diagnosis of osteoporosis? J Nucl Med 48 (Suppl.2):127P,2007.

10. Koopmans KP, De Groot J, Kema IP, Plukker JT, Links TP, **Jager PL.** Value of ^{18}Fluoro-L-DOPA PET in the follow-up of patients with biochemical evidence of medullary thyroid cancer. J Nucl Med 48(Suppl.2):154P,2007

11. Koopmans KP, De Vries EGE, Kema IP, **Elsinga PH, Neels OC,** Sluiter WJ, Vanghillewe K, **Brouwers AH, Jager PL.** ^{11}C-5-HTP and ^{18}F-DOPA PET superior for staging carcinoid and islet cell tumors. J Nucl Med 48(Suppl.2):153P,2007

12. Krabbe C, Dijkstra P, **Pruim J,** Van der Laan B, Van der Wal J, Gravendeel J, Roodenburg J. Value of FDG PET for confirmation of N0 neck and detection of occult metastases in oral and oropharyngeal cancer. Oral Oncology 2(Suppl S):144,2007

13. Krug B, **Van Zanten A,** Pirson A, Crott R, Vanderborght T. Activity-based costing evaluation of [^{18}F]-Fluorodeoxyglucose Positron Emission Tomography study. Eur J Nucl Med Mol Imaging 34(Suppl 2):S241,2007.

14. **Neels OC,** Kema IP, **Jager PL, Koopmans KP,** De Vries EGE, **Dierckx RA, Elsinga PH.** [^{18}F]-5-Fluoroindole: A novel precursor towards the enzymatic synthesis of fluorine-18 labelled tryptophan. J Label Comp Radiopharm 50(Suppl 1):S148,2007

15. **Neels OC,** Timmer-Bosscha H, Kema IP, **Koopmans KP, Jager PL,** De Vries EGE, **Dierckx RA, Elsinga PH.** [^{11}C]5-http and [^{18}F]FDOPA: A view on uptake mechanisms and metabolism in a neuroendocrine pancreas tumour cell line. J Label Comp Radiopharm 50(Suppl 1):S484,2007

16. **Phan HT, Jager PL,** Plukker JT, Wolffenbuttel BH, **Dierckx RA,** Links TP. The diagnostic value of ^{124}I-PET in patients with differentiated thyroid cancer. J Nucl Med 48(Suppl.2):68P,2007

17. Roodenburg JLN, **Pruim J,** Prost WJ, De Bree R, Van den Hoogen FJA, Van der Werff-Regelink G, Hoekstra OS, Marres HAM, Van der Laan BFAM, Oyen WJG. Cost-effectiveness of FDG-PET for the detection of unknown primary tumours presenting as a lymph node metastasis in the neck. Oral Oncology 2(Suppl S):70,2007.

18. Roodenburg JLN, **Pruim J,** Prost WJ, De Bree R, Van den Hoogen FJA, Van der Werff-Regelink G, Hoekstra OS, Marres HAM, Van der Laan BFAM, Oyen WJG, Van der Hilst CS, Leeman CR. Cost-effectiveness of FDG-PET for the detection of unknown primary tumours presenting as a lymph node metastasis in the neck. Oral Oncology 2(Suppl S):99,2007.

19. Van Marle S, **Elsinga PH, Willemsen AT, Van Waarde A, Maas B, Dierckx RA,** Timmerman W, Van Vliet A, Yoshikawa K, Takao K, Mita S, Kimura Y, Ishiwata K, Kobayashi T. A PET study to assess the pharmacokinetics and sigma receptor occupancy in brain of SA4503 at three dose levels in healthy male volunteers. Int Proc Eur Assoc Clin Pharmacol Ther, 8th Congress, 39-42, 2007

20. **Van Waarde A**. Analysis of radiopharmaceutical metabolism. [invited lecture, CME8: Radiopharmacy, Pharmacokinetic modeling]. Eur J Nucl Med Mol Imaging 34(Suppl 2):S191,2007.

21. **Van Waarde A, De Jong JR,** Ishiwata K, **Dierckx RA, Elsinga PH.** Micro-PET imaging and tumor cell binding studies of sigma receptor ligands: A comparison with metabolic PET tracers. J Label Comp Radiopharm 50(Suppl 1):S280,2007.

22. **Van Waarde A, De Jong JR,** Ishiwata K, **Dierckx RA, Elsinga PH.** Early changes of FDG and sigma ligand uptake in rat gliomas after in vivo treatment with doxorubicin. J Label Comp Radiopharm 50(Suppl 1):S281,2007.

23. **Van Waarde A,** Shiba K, **De Jong JR,** Ishiwata K, **Dierckx RA, Elsinga PH.** Rapid reduction of sigma-1 receptor binding and FDG uptake in rat gliomas after in vivo treatment with doxorubicin. Eur J Nucl Med Mol Imaging 34(Suppl 2):S222-S223,2007.

24. Verhoef CC, Groen H, Van Dullemen HM, **Jager PL,** Van der Jagt EJ, Plukker JT. Centralized implementation of accurate and efficient preoperative staging in esophageal cancer patients. Ann Surg Oncol 14 (Suppl S):71-72, 2007.

5.7 Conference proceedings, lectures, etc.

1. **Brouwers AH.** "Nucleaire diagnostiek bij het feochromocytoom". Refereeravond Endocrinologie, Groningen 2007.

2. **Brouwers AH.** "Waarde van FDG-PET bij het cholangiocarcinoom: ervaring van het UMCG". Refereermiddag MDL, 2007.

3. Dasselaar J, **Lub-de Hooge MN, Pruim J, Nijnuis H,** Wiersum A, De Jong PE. "Relative blood volume changes underestimate absolute blood volume changes during hemodialysis". Voordracht, Nederlandse Nefrologiedagen, 3 april 2007.

4. Dasselaar J, **Lub-de Hooge MN, Pruim J, Nijnuis H**, Wiersum A, De Jong PE. "Relative blood volume changes underestimate absolute blood volume changes during hemodialysis". Oral presentation, Congres ERA-EDTA, Barcelona, Spain, June 21-24, 2007.

5. **De Jong JR.** "Animal PET/SPECT/CT". Invited lecture, Refereeravond Nucleaire Geneeskunde Noord-Nederland, Groningen, November 27, 2007.

6. **De Jong JR.** "Small animal scanners: PET, SPECT, CT". Workshop PET voor klinisch fysici (i.o.), UMCG, October 4-5, 2007

7. **De Vries EFJ, Doorduin J, Van Waarde A, Dierckx RA.** "Radiolabeled COX-2 inhibitors as probes for PET imaging". Abstract, TOPIM'07 (Hot Topics in Molecular Imaging: Imaging of Neuroinflammation and Neurodegeneration), Les Houches, France 2007.

8. **De Vries EFJ, Van Waarde A, Willemsen ATM,** Wesselius A, De Groot DMG. "Functional imaging of developmental neurotoxicity". Abstract, 24th International Neurotoxicology Conference, San Antonio, TX, USA, November 11-14, 2007 [microPET study performed in cooperation with TNO Zeist]

9. **Dierckx RA.** "The Future of Molecular Imaging: Concluding Remarks". Invited lecture, International Symposium on Molecular Imaging for Diagnosis and Prediction of Treatment Outcome, Groningen, Netherlands, September 14, 2007.

10. **Dierckx RA.** "De bijdrage van de nucleaire geneeskunde aan de evaluatie en behandeling van sportletsels", Congres Sportgeneeskunde, Amsterdam, Netherlands, November 30, 2007.

11. **Dieckx RA.** "PET diagnostiek van het feochromocytoom". Symposium Endocrinologie, UMCG, Groningen, Netherlands, December 11, 2008.

12. **Dijkers ECF. "**Characterization of ^{89}Zr-trastuzumab for clinical HER2 immunoPET imaging". Oral presentation, abstract # 3508, Annual Meeting, American Society of Clinical Oncology, Chicago IL, USA, 2007.

13. **Doorduin J, Klein HC,** James M, Kassiou M, **Dierckx RA, De Vries EFJ. "**PET imaging of peripheral benzodiazepine receptors in a rat model of herpes encephalitis". Abstract, TOPIM'07 (Hot Topics in Molecular Imaging: Imaging of Neuroinflammation and Neurodegeneration), Les Houches, France 2007.

14. **Elsinga PH. "**Drug design of PET-tracers". Imperial GSK PET-course, London, UK, 2007.

15. **Elsinga PH. "**PET-studies of P-glycoprotein function in the brain". Cerebral Vascular Biology Symposium, Ottawa, Canada, 2007

16. **Elsinga PH. "**Imaging of Myocardial Beta-Adrenoceptors Using (S)-[^{11}C]CGP 12388 and PET: Radiosynthesis, In vivo Characterization, Modeling, and Human Studies", Lecture, Ottawa Heart Institute, Ottawa, Canada, 2007

17. **Elsinga PH. "**Radiopharmaceutical Chemistry in Groningen", Lecture, McMaster University, Hamilton, Canada, 2007

18. **Elsinga PH. "**Drug design", Continuing Medical Education Radiopharmacy Committee, EANM, Copenhagen, Denmark, October 2007

19. **Elsinga PH.** College Organische Chemie, 3e jaars studenten Scheikunde, Rijksuniversiteit Groningen 2007

20. **Klein HC.** "Pathophysiology of Schizophrenia: Neuroinflammation?". Invited lecture, International Symposium on Molecular Imaging for Diagnosis and Prediction of Treatment Outcome, Groningen, Netherlands, September 14, 2007.

21. **Koopmans KP.** "Imaging of Neuroendocrine Tumors". Invited lecture, International Symposium on Molecular Imaging for Diagnosis and Prediction of Treatment Outcome, Groningen, Netherlands, September 13, 2007.

22. Krabbe CA, Dijkstra PU, **Pruim J,** Van der Laan BFM, Van der Wal JE, Gravendeel JP, Roodenburg JLN. "Value of FDG PET for Confirmation of N0 Neck and Detection of Occult Metastases in Oral and Oropharyngeal Cancer". First World Congress of the International Academy of Oral Oncology, Amsterdam, Netherlands, May 17-20, 2007

23. Kristanto W, Dikkers R, Van Ooijen PMA, Greuter MJW, Willems TP, Oudkerk M. "Morphological atherosclerotic plaque analysis on coronary artery autopsy specimens using dual source computed tomography, micro computed tomography, and histopathology". Poster presentation, European Congress of Radiology, Vienna, Austria, March 9-13, 2007 *[microCT was used for this presentation]*.

24. **Lazarenko S.** "HD-PET". Invited lecture, Refereeravond Nucleaire Geneeskunde Noord-Nederland, Groningen, November 27, 2007.

25. **Lub-De Hooge MN.** "Monoclonal Antibodies in Diagnosis and Therapy". Invited lecture, International Symposium on Molecular Imaging for Diagnosis and Prediction of Treatment Outcome, Groningen, Netherlands, September 14, 2007.

26. **Nagengast WB**, De Vries EGE, Hospers GAP, Mulder NH, **De Jong JR, Brouwers AH, De Hooge MN**. "In vivo VEGF imaging with ^{89}Zr-bevacizumab in a human ovarian xenograft model using microPET and microCT". Abstract, Annual Meeting, American Association for Cancer Research, Los Angeles CA, USA 2007.

27. Paans AMJ. "PET + CT: What is Next?" Invited lecture, International Symposium on Molecular Imaging for Diagnosis and Prediction of Treatment Outcome, Groningen, Netherlands, September 14, 2007.

28. Paans AMJ. College Nuclear Medicine: "PET and SPECT", voor 2e jaars studenten Life Science & Technology, Groningen 2007.

29. Paans AMJ. "PET scanners". Workshop PET voor klinisch fysici (i.o.), UMCG, October 4-5, 2007

30. Paans AMJ. "Future developments in the field of nuclear imaging". Workshop PET voor klinisch fysici (i.o.), UMCG, October 4-5, 2007

31. Paans AMJ. "Positron Emissie Tomografie". 6e leergang Stralingsbescherming en Dosimetrie, 2007.

32. Paans AMJ, Pruim J, Sturkenboom MGG, De Vries EFJ, Van Waarde A (secr.) "Molecular Imaging for Diagnosis and Prediction of Treatment Outcome" – organisatie van dit internationaal symposium met ca. 200 deelnemers, ter gelegenheid van "30 Jaar PET in Groningen", September 13-14, 2007.

33. Paans AMJ, Lazarenko S, Wierts R. College/werkcollege "Radioactivity and Imaging" voor 1e en 2e jaars studenten Life Science & Technology, Groningen 2007

34. Phan TTH. "The Diagnostic Value of ^{124}I-PET in Patients with Differentiated Thyroid Cancer". Invited lecture, International Symposium on Molecular Imaging for Diagnosis and Prediction of Treatment Outcome, Groningen, Netherlands, September 14, 2007.

35. Slart RHJA. "Myocardial viability assessed with nuclear medicine techniques". Voordracht CVOI, Nederlandse Vereniging voor Cardiologie, Utrecht, October 2007.

36. Slart RHJA. Symposium "Oncologische Beeldvorming" voor studenten Levenswetenschappen. Department of Biology, University of Groningen, Haren 2007.

37. Slart RHJA. Introductory course on nuclear medicine for students of medicine (part of the requirements for the M.D. degree. Groningen 2007

38. Van Waarde A. "Effects of animal handling on the outcome of microPET studies." Invited lecture, 6th Workshop Radiochemie.NL, Rijksuniversiteit Groningen, Groningen, January 19, 2007.

39. **Van Waarde A.** "PET imaging of transport processes in living animals and humans". *Course on Membranes, Signal Transduction and Transport*, Graduate School GUIDE, Groningen, March 16, 2007.

40. **Van Waarde A. "**Metabolism of positron-emitting radiopharmaceuticals: Plasma metabolite analysis". Invited lecture, Continuing Medical Education, European Association of Nuclear Medicine, Copenhagen, Denmark, October 2007

41. **Wierts R.** "Time-of-flight PET". Invited lecture, Refereeravond Nucleaire Geneeskunde Noord-Nederland, Groningen, November 27, 2007.

42. **Willemsen ATM.** "Pharmacokinetic modeling". Workshop PET voor klinisch fysici (i.o.), UMCG, October 4-5, 2007

5.8 Book Chapters

1. Schröder CP, Hospers GAP, Willemse PHB, Perik PJ, **De Vries EFJ, Jager PL,** Van der Graaf WT, **Lub-De Hooge MN,** De Vries EGE. Molecular Imaging in Metastatic Breast Cancer. Chapter 15 in: Mansel RE et al. (eds). Metastasis of Breast Cancer, Berlin: Springer Verlag 2007, pag.307-319.

PERSONNEL

Listed by function in alphabetic order

6.1 Medical Staff

Ali Agool MD
Adrienne H Brouwers MD PhD
Prof. Rudi A.Dierckx MD PhD (Head of the Department)
Andor Glaudemans MD
Pieter L Jager MD PhD
Ha Phan MD (until Nov 1, 2007)
Jan Pruim MD PhD
Riemer HJA Slart MD PhD

6.2 Residents-in-Training

Sylvia Eshuis MD
Klaas Pieter Koopmans MD PhD
Niels Veltman MD

6.3 Medical Physics

Johan R de Jong PhD (medical physicist-in-training)
Sergiy Lazarenko PhD (medical physicist-in-training)
Prof Anne MJ Paans PhD (medical physicist)
Klaas Willem Sietsma (system administrator)
Roel Wierts (physicist-in-training)
Antoon TM Willemsen PhD (medical physicist)

6.4 Radiochemistry

Joost Bruns (lab technician)
Hilde Dekens (lab technician)
Philip H.Elsinga PhD (radiochemist)
Lizette Eriks (lab technician)
Chris Harms (lab technician)
Marissa Heijnen (assistant)
Kirsten Huisstede (lab technician)
Peet Joosten (lab technician, left in 2007)
Chantal Kwizera (lab technician)
Vanathee Logendran (assistant)
Marjolijn Lub-de Hooge PhD (pharmacist)
Bram Maas (lab technician)
Jitze Medema (lab coördinator / technician)
Yvonne J Moedt (assistant, left in 2007)
Hugo Nijnuis (lab coördinator / technician)
Esther Olthoff (assistant)
Frieda Pelleboer (assistant, left in 2007)
Hans Pol (lab technician)
Marieke Sturkenboom MSc (pharmacist)
Bertha Tamming (lab technician)
Erik FJ de Vries PhD (radiochemist)
Michel de Vries (lab technician)

Aren van Waarde PhD (biochemist)

6.5 Nuclear Medicine Technologists

Marijke Broersma
José E Douma
Sharon Jonkman (left on Sept 1, 2007)
Yvonne AM van der Knaap
Remko Koning
Clara Lemstra
Bregtsje Negenman
Yvonne Reitsma
Eelco Severs
Jurgen Sijbesma (biotechnician)
Paul van Snick
Hans ter Veen (coordinator)
Hedy C Vrakking
Johan Wiegers
Aafke Zeilstra

6.6 Medical & Financial Administration

Arja RJ Hoekman
Ilse Sewnandan
Hanna van der Sloot
Alice Staal-Kloosstra (left in 2007)
Gerda J de Voogd
Rika C van der Werff
Erna R van der Wijk
Annie K van Zanten ML

6.7 PhD Students

Janine Doorduin MSc
Inês Farinha Antunes MSc
Reza Golestani MD
Onno L de Klerk MD
Silvana Kruizinga MSc
Leila Mirfeizi MSc
Oliver L.Neels MSc
Anna Rybczynska MSc

6.8 Visiting Scientists

Alessio Annovazzi MD (Roma)
Marco Chianelli MD PhD (Roma)
Hans C Klein MD PhD (Winschoten)
Prof. Alberto Signore MD (Roma)
Prof. Johan De Sutter MD PhD (Ghent)
Prof. Christophe van de Wiele MD PhD (Ghent)

6.9 Scientific staff and graduate students from GUIDE, BCN and other departments participating in imaging studies

Dr. H.Bijl, radiotherapy
Dr. M.Bijl, clinical immunology
Prof. Dr. R.P.H.Bischoff, analytical biochemistry
Prof. Dr. H.W.G.M.Boddeke, medical physiology
Prof. Dr. J.A.den Boer, psychiatry
Dr. F.J.Bosker, psychiatry
Drs. A.J.Breeuwsma, urology
Dr. B.Buwalda, animal physiology
Dr. R.P.Coppes, radiology
Dr. J.C.V.M. Copray, medical physiology
Dr. R.P.F.Dullaart, endocrinology
Dr. H.M.van Dullemen, gasteroenterology
Dr. M.J.W.Greuter, radiology
Prof. Dr. H.J.M.Groen, pulmonology
Dr. D.M.G.de Groot, TNO-Quality of Life, Zeist
Prof. Dr. H.J.Haisma, pharmacokinetics & drug delivery
Prof. Dr. J.M.M.Hooymans, ophthalmology
Prof. Dr.G.J.ter Horst, BCN
Drs. A.N.A.van der Horst, endocrinology
Drs. J.C.C.van der Horst, cardiology
Dr. G.A.P.Hospers, medical oncology
Dr. E.J.van der Jagt, radiology
Dr. B.M.de Jong, neurology
Dr. I.J. de Jong, urology
Dr. R.M. de Jong, cardiology
Dr. S.de Jong, medical oncology
Drs. M.M.G.J.Jongen, urology
Dr. I.P.Kema, laboratory medicine
Dr. R.Kortekaas, anatomy & embryology
Dr. J.G.W. Kosterink, pharmacy
Dr. T.van Laar, neurology
Prof.Dr. K.L.Leenders, neurology
Prof.Dr.L.F.M.H. de Leij, GUIDE
Dr. T.P.Links, endocrinology
Prof.Dr. P.G.M.Luiten, animal physiology
Dr. P.van Luijk, radiotherapy
Dr. P.Meerlo, animal physiology
Dr. J.Meijer, medical oncology
Prof.Dr.H.Moshage, GUIDE
Prof.Dr. N.H.Mulder, medical oncology
Drs. J.C.H.van Oostrom, neurology
Prof.Dr. M.Oudkerk, radiology
Dr. J.T.M.Plukker, surgical oncology
Dr. M.G.Rots, pharmacokinetics & drug delivery
Dr. W.J.Sluiter, pathology & laboratory medicine
Prof.Dr. M.J.Staal, neurosurgery
Drs. M.Stam, radiotherapy
Dr. A.J.H.Suurmeijer, pathology & laboratory medicine
Dr. R.A.Tio, cardiology
Prof. Dr. D.J.van Veldhuisen, cardiology
Drs. C.C.Verschuuren, clinical genetics
Drs. P.A.van der Vleuten, cardiology

Prof.Dr. E.G.E.de Vries, medical oncology
Dr. J.Wesseling, pathology & laboratory medicine
Prof.Dr. T.Wiggers, surgery
Prof.Dr. B.H.R.Wolffenbuttel, endocrinology
Prof.Dr. F.Zijlstra, thorax center
Prof.Dr. A.G.J.van der Zee, gynaecology

OTHER RESPONSIBILITIES

7.1 Teaching activities

Staff members of NMMI were involved in, or contributed to, the following teaching activities:

College “Nucleaire Geneeskunde”, voor farmacie studenten in kader van cursus Inleiding Ziekenhuisfarmacie
College “Nuclear Medicine (PET and SPECT)”, 2e jaars studenten Life Science and Technology, Groningen
College “Organic Chemistry” voor 3e jaars studenten Scheikunde, Groningen
College “Radioactivity and Imaging”, 1e jaars studenten Life Science and Technology, Groningen
Course on “Membranes, Signal Transduction and Transport”, Graduate School GUIDE, Groningen, March 16, 2007
European Association of Nuclear Medicine, Continuing Medical Education, Radiopharmacy Committee, Copenhagen, Denmark
Imperial GSK PET Course, London, UK
International Symposium on “Molecular Imaging for Diagnosis and Prediction of Treatment Outcome”, Groningen, Sept 13 and 14, 2007
Introductory Course on Nuclear Medicine, voor studenten geneeskunde, Groningen
Leergang Stralingsbescherming en Dosimetrie, no.6
Nederlandse Nefrologiedagen, April 3, 2007
Nederlandse Vereniging voor Cardiologie, CVOI, Utrecht
Refereeravonden Endocrinologie, UMCG, Groningen
Refereeravonden Nucleaire Geneeskunde Noord-Nederland
Refereermiddag Maag-Darm-Lever artsen
Symposium Oncologische Beeldvorming voor studenten Levenswetenschappen, Haren 2007
Workshop PET voor klinisch fysici, October 4 and 5, 2007
Workshop Radiochemie.NL, Groningen, January 19, 2007

To celebrate the fact that the first PET images in Groningen were made 30 years ago, the Department of NMMI organized an international symposium (2 days, about 200 participants) entitled: “**Molecular Imaging for Diagnosis and Prediction of Treatment Outcome”.** The symposium was organized by R.A.Dierckx, A.M.J.Paans, J.Pruim, M.G.G.Sturkenboom, G.J.de Voogd, E.F.J.de Vries and A.van Waarde, with external support from S.J.Klont. Industrial sponsors were: Siemens, GE Healthcare, Tyco Healthcare, Philips and Von Gahlen. Speakers were: R.Baum (Bad Berka), F.Bengel (Baltimore), J.A.den Boer (Groningen), L.Brepoels (Leuven) D.J.Brooks (London), I.Carrio (Barcelona, Editor-in-Chief of the European Journal of Nuclear Medicine and Molecular Imaging), A.Cuocolo (Naples, President of the European Association of Nuclear Medicine), V.J.Cunningham (London), W.Enghardt (Dresden), R.Z.Goldstein (Upton, NY), K.Herholz (Manchester), H.R.Herschman (Los Angeles), L.Hofstra (Maastricht), I.J.de Jong (Groningen), K.P.Koopmans (Groningen), K.L.Leenders (Groningen), M.Lub-de Hooge (Groningen), H.Minn

(Turku), A.M.J.Paans (Groningen), S.N.Reske (Ulm), E.G.E.de Vries (Groningen), and C.van de Wiele (Ghent).

7.2 Appointments, diploms, (inter) national cooperation

In August 2007, Ing.J.W.A.Sijbesma was appointed as biotechnican and general manager of the facilities for small animal imaging (microPET and microCT).

7.3 Social responsibilities

Algemeen Stralings Deskundige, Universitair Medisch Centrum Groningen (A.M.J.Paans)
Chairman, Radiochemie.NL (Dutch Society of Radiopharmaceutical Chemistry) (P.H.Elsinga)
European Editor, Nuclear Medicine Communications (R.A.Dierckx)
Executive Guest Editor on PET and SPECT in Drug Design, Current Pharmaceutical Design (A.van Waarde)
Lid, Beoordelingscommissie (20 proefschriften, R.A.Dierckx)
Lid, Beoordelingscommissie (3 proefschriften, A.M.J.Paans)
Lid, CBO richtlijn ontwikkeling Hypopharynxcarcinoom (namens de Nederlandse Vereniging voor Nucleaire Geneeskunde (J.Pruim)
Lid, Commissie Kwailiteit Bevordering, Nederlandse Vereniging voor Nucleaire Geneeskunde (A.H.Brouwers)
Lid, Commissie Voorziening Kernenergiewet, Nederlandse Vereniging voor Nucleaire Geneeskunde (A.M.J.Paans)
Lid, Concilium, Nederlandse Vereniging voor Nucleaire Geneeskunde (R.A.Dierckx)
Lid, Disciplinegroep Medische Beeldvorming, Stichting Kinderoncologie Nederland (A.H.Brouwers)
Lid, FONA commissie, Universitair Medisch Centrum Groningen (M.N.Lub-De Hooge)
Lid, IKN Werkgroep Schildkliertumoren (P.L.Jager)
Lid, Medisch-Ethische Toetsings Commissie, Universitair Medisch Centrum Groningen (A.M.J.Paans)
Lid, Netwerk Nederlands Kenniscentrum voor Farmacotherapie bij Kinderen (M.N.Lub-De Hooge)
Lid, Onderwijscommissie, Nederlandse Vereniging voor Nucleaire Geneeskunde (J.Pruim)
Lid, Redactie Leerboek Nucleaire Geneeskunde (C.Lemstra)
Lid, SIG Kindergeneeskunde, Nederlandse Vereniging van Ziekenhuis Apothekers (M.N.Lub-de Hooge)
Lid, Stuurgroep Ontwikkeling Zorgtraject (Bij)Schildklier, Universitair Medisch Centrum Groningen (A.H.Brouwers)
Lid, Visitatiecommissie Nederlandse Vereniging voor Nucleaire Geneeskunde (R.A.Dierckx, P.L.Jager)
Lid, Werkgroep Atriumfibrilleren, Proeftuin Groningen t.b.v. Groninger Transmuraal Formularium (M.N.Lub-De Hooge)
Lid, Werkgroep Nederlandse Federatie van Universitaire Ziekenhuizen (R.A.Dierckx)
Member, Board of Directors, International Society of Radiopharmaceutical Sciences

(P.H.Elsinga)
Member, Board International Research Group in Immuno-Scintigraphy and Therapy (IRIST) (M.N.Lub-De Hooge)
Member, Committee on Radiopharmacy, European Association of Nuclear Medicine (P.H.Elsinga)
Member, Editorial Board, European Journal of Nuclear Medicine and Molecular Imaging (R.A.Dierckx)
Member, HOVON Imaging work group (J.Pruim, A.T.M.Willemsen)
Opleider Klinische Fysica (A.M.J.Paans)
Opleider Nucleaire Geneeskunde (R.A.J.O.Dierckx)
Opleider Nucleaire Geneeskunde (J.Pruim)
Secretaris Maatschappelijke Zaken, bestuur Nederlandse Vereniging voor Nucleaire Geneeskunde (A.M.J.Paans)
Teacher, Annual Course on PET/CT, European Association of Nuclear Medicine, Vienna (J.Pruim)
Voorzitter, SIG Nucleaire Geneeskunde en Radiofarmacie, Nederlandse Vereniging van Ziekenhuis Apothekers (M.N.Lub-De Hooge)